[American Journal of Science, Vol. 304, April, 2004, P. 333–369]

EXTRA-BASINAL FLUID INFILTRATION, MASS TRANSFER, AND VOLUME STRAIN DURING FOLDING: INSIGHTS FROM THE IDAHO-MONTANA THRUST BELT

DAVID J. ANASTASIO*, GRAY E. BEBOUT*, and JAMES E. HOLL†

*Department of Earth and Environmental Sciences, Lehigh University, Bethlehem, Pennsylvania, 18015; dja2@lehigh.edu; geb0@lehigh.edu

ABSTRACT. Finite strain and geochemical variations along strain gradients were used to study cleavage development in carbonates in the Lost River Range, Idaho. Deformation accommodating layer-parallel shear was partitioned into thin deformation zones during folding of Willow Creek anticline. Cleavage intensity is strong to very strong in deformation zones and weak in surrounding rocks. Strain magnitudes range from $\bar{e}_s$=0.32 (1.15:0.93:0.73; x, y, z, principal axes of strain) outside, to $\bar{e}_s$=0.64 (1.29:0.80:0.52) inside, deformation zones. We found a positive linear correlation between strain, cleavage development, and negative dilation. Volume loss, at a cubic centimeter scale, ranges from 12 percent to 49 percent. Cleavage selvages are depleted in Ca and ^{18}O and enriched in other elements relative to microlithons and less deformed protolith carbonates. Mass-balance considerations indicate that cleavage was formed by incongruent pressure solution leading to a passive concentration of less soluble components during Ca loss and metasomatic additions of Si, Al, and K to produce authigenic clay minerals in selvages.

Data for the Willow Creek locality and elsewhere in the Lost River Range (Davidson and others, 1998), Pioneer Mountains, and the Tendoy Range (Bebout and others, 2001), show that across the Sevier orogen, fluid infiltration was heterogeneous at centimeter-kilometer scales and resulted from positive feedback between deformation and far-traveled surficial fluids. Metasomatic strain softening enhanced deformation zone development, which generated increased permeability as the thrust belt evolved from a porosity-based closed system to a discontinuity-based open system. Increased fluid infiltration and isotopic exchange was associated with volume loss, increasingly prolate strains, and crystallization of clays, to produce the cleavage selvages. Mass transfer was accommodated by diffusion early and advection later in the deformation history. Mesoscopic structures (deformation zones, faults, veins) focused fluid flow and were kinematically related to larger-scale structures (faults, fault-related folds). The inferred addition of surficial fluids to depths of >7 kilometers in the thrust belt implies a fluid regime involving significant topographically driven recharge. Deformed whole-rocks and microsamples are lower in $\delta^{18}O$ than undeformed samples which have O- and C-isotope compositions similar to those of marine carbonates. Veins are even lower in $\delta^{18}O_{V\text{-}SMOW}$, with minimum values of $\sim+5$ permil reflecting penetration of the crust by ocean-derived precipitation with $\delta^{18}O$ near to somewhat lower than 0 permil (range of -7.5 to $+2.5‰$ calculated for H_2O in equilibrium with these veins). The inferred penetration, into the thrust belt, of nearshore meteoric waters is consistent with proximity to the reconstructed Western Interior Seaway. Later fluid infiltration locally lowered the $\delta^{18}O$ of carbonates even further, based on the O-isotope compositions of veins related to younger compressional deformation and to the onset of crustal-scale extension in the Eocene. This progression toward lowered $\delta^{18}O$ of the surficial waters is compatible with the retreat of the seaway during emergence of the thrust wedge and Paleogene extension, uplift, and subaerial volcanism.

INTRODUCTION

Fluids play an integral role in orogenic dynamics (Hubert and Rubey, 1959; Davis and others, 1983; Forster and Smith, 1990), the earthquake cycle (Sibson, 1981, 1990),

†Current address: Exxon-Mobil Upstream Development Company, Houston, Texas, 77252

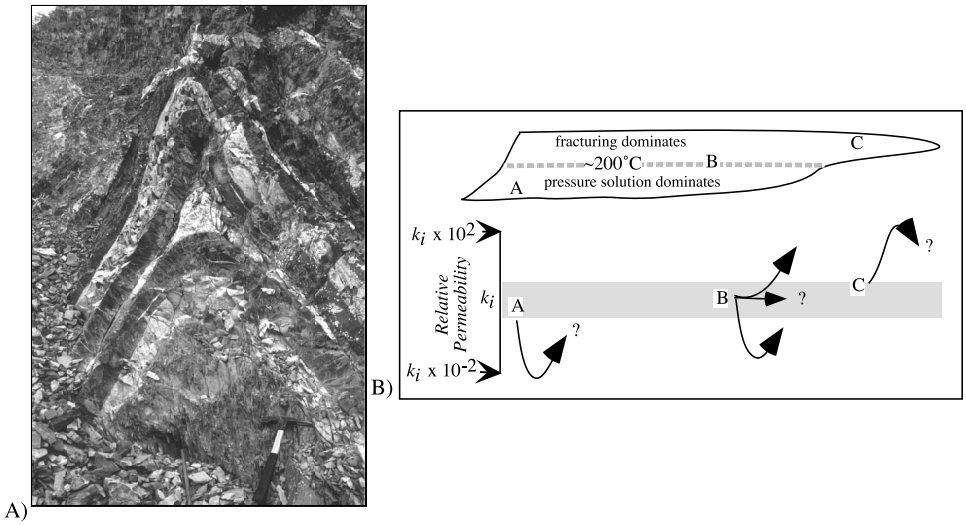

Fig. 1. Deformation mechanisms and mass transfer. (A) Field photograph of the core of the Willow Creek anticline at the level of the Middle Canyon Formation showing a well-developed cleavage in the inner fold arc and saddle-reef veins along the outer fold arc of several beds illustrating local mass transfer and dilation variation. Rock hammer for scale. (B) Schematic carbonate thrust sheet showing the domains dominated by fracturing and pressure solution, respectively, illustrating potential permeability variations accompanying deformation.

mass and heat transfer during deformation (Kerrich, 1986; Garven, 1989; Bethke and Marshak, 1990; Ge and Garven, 1994; Bachu, 1995; Machel and others, 1996), and the generation of hydrocarbon and epigenetic ore deposits (Oliver, 1986; Sverjensky, 1986; Duane and de Wit, 1988). Deformation features such as cleavage and veins, which coincide in space and time attest to the important role fluid accommodated mass transfer plays in deformation. Over a range of scales, deformation results in coeval positive and negative dilations, which impact fluid-rock interactions in heterogeneous ways (fig. 1). Depending on lithology and position within the orogenic wedge, the dominant deformation mechanism(s) and strain history will vary and consequently so will fluid pathways, becoming enhanced in some parts of the belt and diminishing in others. For example, in carbonates at temperatures above 200°C (Holl and Anastasio, 1995) or in siliclastics at 300°C or higher (Elliott, 1976), pressure solution is recognized as the most important porosity reducing mechanism during deformation leading to stylolites and sutured and truncated grain contacts.

The impact of fracturing and vein formation on fluid flow in thrust belts depends on fracture type, orientation, timing with respect to other competing deformation mechanisms, and the opening and filling history (Mitra, 1987). In general, fracture abundance and attendant permeability enhancement, increase towards the synorogenic surface and towards the foreland, where environmental conditions favor brittle deformation. However, where intense and localized fracturing leads to cataclasis a permeability reduction can occur. Because discontinuities such as cleavage zones, fractures, and faults evolve texturally and chemically during progressive deformation, coupled analysis of deformation and fluid-rock interactions are required to identify important feedback mechanisms. Furthermore, the relative importance of permeability enhancing mechanisms (fracturing) and permeability decreasing mechanisms (pressure solution, cataclasis) varies spatially as well as temporally within the thrust wedge. In the hinterland, understanding strain and mass transfer is complicated by uncertain volume fluxes.

In orogenic forelands, pressure solution results in the majority of penetrative strain (Alvarez and others, 1978; Holl and Anastasio, 1995), controls the rheology of thrust sheets (Elliott, 1976) and is the principal mechanism of cleavage formation in slates (Sorby, 1853; Plessman, 1965), sandstones (Nickelson, 1972; Geiser, 1974; Gray, 1978) limestones (Nickelson, 1972; Groshong, 1975; Alvarez and others, 1978; Engelder and Marshak, 1985; Meyer and Dunne, 1990) and dolomite (Schweitzer and Simpson, 1986; Knipe, 1989). A long accepted model of cleavage formation in carbonates (that is, Alvarez and others, 1978; Engelder and Marshak, 1985; DePaor and others, 1991) holds that as carbonate minerals preferentially dissolve and are removed from a local system by diffusion (Durney, 1972; Elliott, 1973; Mitra, 1976; Rutter, 1983; Kerrich, 1986) or flow (Cox and Etheridge, 1989), less soluble components such as phyllosilicates, Fe-oxides, and organic matter are passively concentrated in selvage zones to form the disjunctive fabric. Mass transfer out of selvages and local precipitation in pore spaces, strain shadows, or vein arrays (Durney, 1972; Durney and Ramsay, 1973; Means, 1975; Williams, 1977; Beach, 1977; Ramsey, 1980; Cox and Etheridge, 1989) or long-range mass transport (Alvarez and others, 1978; Wright and Platt, 1982; Beutner and Charles, 1985; Wright and Henderson, 1992; Fisher and Brantley, 1992) has been proposed to explain the enrichment in elements such as Al and Ti relative to the concentrations of these elements in uncleaved or less metamorphosed rock (for example, Engelder, 1984; Erslev and Ward, 1994; Ague 1991, 1994).

Previous assessments of volume flux during cleavage formation have yielded contradictory results. In general, strain-based structural interpretations in slates support large-scale volume losses (25–60% over 10's of km^2) associated with cleavage formation (for example, Sorby, 1853; Wright and Platt, 1982; Bell, 1985; Beutner and Charles, 1985; Henderson and others, 1986; Wright and Henderson, 1992; Feehan and Brandon, 1999), however, geochemically-based interpretations have concluded that little net mass transfer occurred (for example, Stephens and others, 1979; Erslev and Mann, 1984; Clifford and others, 1987; Wintsch and others, 1991; Erslev and Ward, 1994). Davidson and others (1998) sought to reconcile this discrepancy by using both geometric and geochemical approaches to study cleavage development in carbonates and concluded that at centimeter to meter scales where strain assessments were homogeneous, geochemical determinations were not; hence the contradictory results. In this paper, we extend earlier work on volume strain and cleavage formation and consider the implications of extra-basinal fluid infiltration in enhancing deformation.

Because of complexities in strain history, which affect the degree and nature of permeability, topographic relief, thrust sheet loading, and the potential for fluid-rock interaction with surficial and deeper reservoirs over long time spans, many possibilities exist concerning the evolution of fluids and fluid pathways during orogenesis (fig. 2). In this study we take advantage of local strain gradients to provide protolith constraints and use both geometrical and geochemical approaches to characterize volume strains during cleavage development and to explore feedbacks between deformation and fluid-rock interaction. Dilations were calculated using bulk strain measurements coupled with direct measurements of principal extension. We use a small number of major and trace element geochemical measurements obtained at the mm- to cm-scales to demonstrate the effects of passive concentration (by pressure solution) and metasomatic additions in leading to cleavage formation in these rocks and a comparison is made with geochemical and geometric volume strain estimates associated with cleavage development in similar rocks (Davidson and others, 1998). Carbon (C) and oxygen (O) stable isotope compositions of cleaved and uncleaved samples, and multiple generations of vein filling, are employed in an assessment of potential fluid sources, fluid compositions, and migration pathways. We combine these data with data from previous Lost River Range studies and data from more foreland sites to evaluate

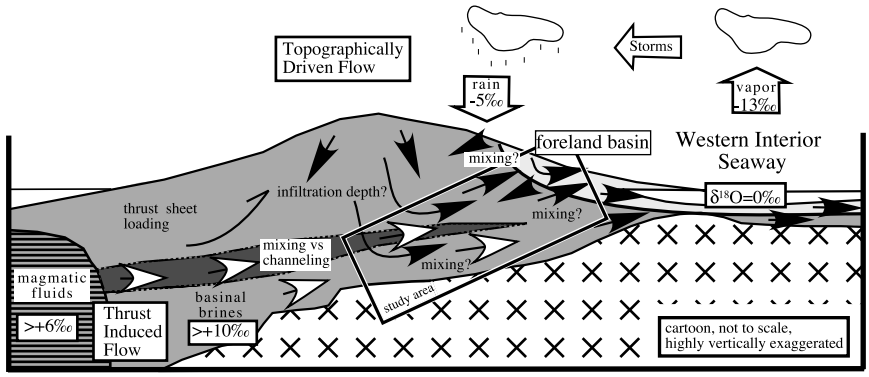

Fig. 2. Schematic illustration of regional-scale fluid flow through an orogenic belt showing fluid sources with $\delta^{18}O_{V\text{-}SMOW}$ values, fluid-driving forces, and the approximate position of rocks investigated in this study. Influenced by Oliver (1986), Garven (1989) and Hutcheon and others (2000). Not to scale, see text for further discussion.

regional-scale synkinematic fluid infiltration in carbonates across the Sevier thrust belt, Montana recess, USA (for example, Davidson and others, 1998; Bebout and others, 2001).

Idaho-Montana Thrust Belt- Stratigraphy and Deformation Conditions

The Sevier thrust belt in southwest Montana and east central Idaho is exposed in the Pioneer and White Knob Mountains and the Lost River, Lemhi, Beaverhead, and Tendoy Ranges (fig. 3). These ranges form parallel NW-SE trending mountains east of the Idaho batholith and north of the Snake River plain. The ranges are separated by extensional half-graben basins, which were active since the Tertiary (Janecke 1992; Anders and others, 1993). Preorogenic strata within the thrust belt consist of a Late Proterozoic-Early Paleozoic rift to passive margin assemblage of clastic and carbonate units up to 3,612 meters thick, deposited on a west-facing shelf. These are overlain by an eastward tapering wedge of Antler flysch (McGowan Creek Formation, 30–1200 m thick), which is in turn overlain by a Late Paleozoic, westerly prograding, carbonate platform 2,506 + meters thick (Link and others, 1988). The late Paleozoic slope is presently located in the White Knob Mountains. In the Lost River Range, substantial Mesozoic section was likely removed subsequent to thrusting based on regional stratigraphic reconstructions of the northern Rockies (Mamet and others, 1971), balanced and restored cross sections across the Wyoming salient (Allmendinger, 1992), and geology and geothermalbarometry within and around the Pioneer Mountains (Dover, 1981; Trepp, ms, 1989; Silverberg, ms, 1990; DePrang, ms, 1997), which all suggest that the Late Paleozoic shelf in the Lost Rir Range restores to a minimum depth of 7 kilometers or more, if likely synorogenic structural thickening and wedge-top deposits are included. This depth is consistent with illite crystallinity analysis of the Scott Peak Formation (Mississippian limestone) in the Lost River Range, which indicates peak metamorphic temperatures of 220°C (Kübler indices average 0.20° 2θ) during Sevier deformation, as well as rare textural evidence (deformation lamellae, subgrains) indicative of dislocation creep in calcite which is thought to require temperatures of ~300°C (Rutter, 1976). In contrast, emergent thrusting and fan delta development along the southwest Montana thrust front suggests deformation near the synorogenic ground surface (Perry and Sando, 1983; Perry and others, 1988; Kulik and Perry, 1988; Williams and Bartley, 1988; Skip and Link, 1992; Schmitt and others, 1995; Anastasio and others, 2002). Vitrinite reflectance and conodont color alteration index

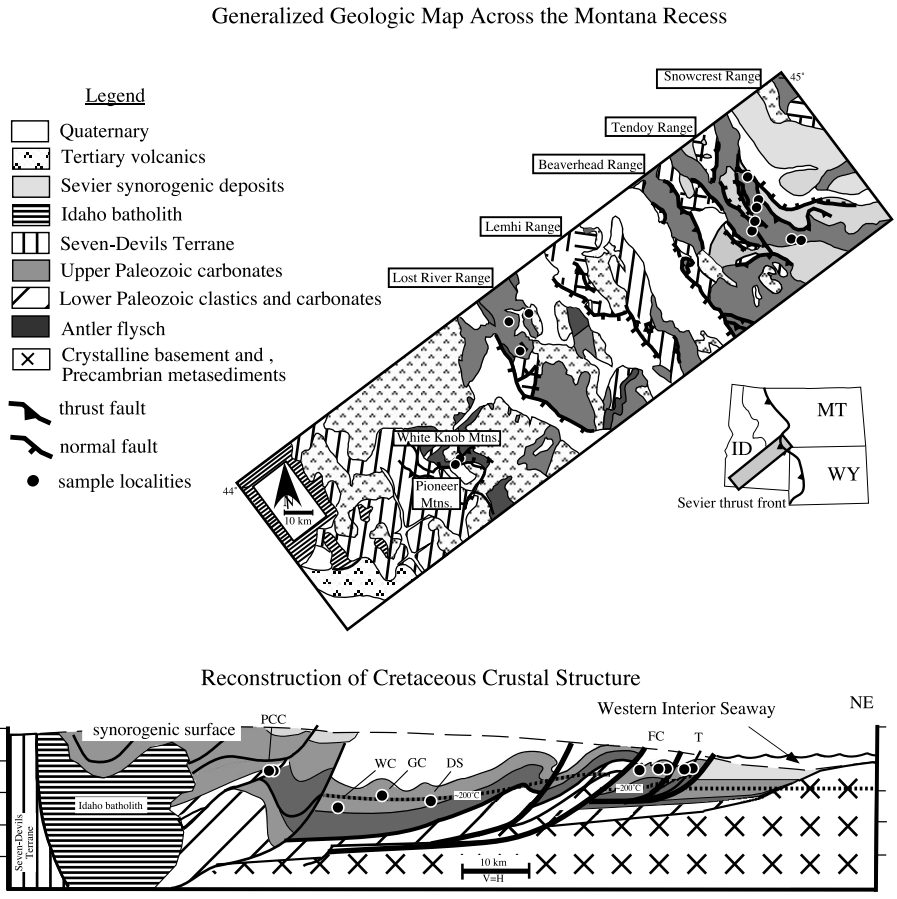

Fig. 3. Generalized geologic map of the study corridor showing sample localities, modified from Skipp and Link (1992), Wilson and Skipp (1994), and Lonn and others (2000). Cross section is a schematic reconstruction of the Sevier thrust belt along the study corridor for the Late Cretaceous, prior to the onset of extension. Constraints on the position, age, and environmental conditions of various positions along the section are described in the text. Sample localities and the predicted position of the 200°C isotherm are shown. PCC-Pioneer Core Complex, WC-Willow Creek anticline, GC-Grouse Creek anticline, DS-Doublesprings duplex, FC-Four Eyes Canyon thrust sheet, T-Tendoy thrust sheet.

values (Perry and others, 1983) and fluid inclusion analysis (Johnson, ms, 2002) support deformation temperatures of 80° to 120°C for the frontal thrust sheets. Intercalated ashes within proximal synorogenic foreland basin conglomerates of the Beaverhead Group constrain emergent thrusting along the thrust front to be Late Cretaceous (79–76 Ma on Erdmont thrust near Bannack, Montana; Kalakay, ms, 2001). Geologic relationships and hornblende cooling ages from the Pioneer Mountains suggest hinterland thrusting 95 to 79 Ma (Silverberg, ms, 1990). The Blacktail-Snowcrest uplift, a foreland Laramide structure, buttressed the frontal thrust sheets resulting in out-of-sequence thrusting within the Montana recess. For example, compressional deformation in the hinterward White Knob Mountains involving the Late Paleozoic slope sequence was active in the middle Eocene (53.6–50.9 Ma, Latta and Anastasio, 2000). Reconnaissance samples containing mechanically twinned carbonate grains from the Lost River Range were used to estimate maximum differential stress magnitudes. The measured frequency of calcite grains with one or multiple sets of mechanical twin

lamellae indicates differential stress magnitudes ranging between 100 to 250 Mpa, using calibrations of Jamison and Spang (1976), values typical of orogenic forelands (for example, Newman, 1994; Holl and Anastasio, 1995).

The structural style varies across the Montana recess of the Sevier thrust belt. Regional folds within the upper Paleozoic carbonates of the Hawley Creek thrust plate (Skipp, ms, 1985), which carries the Lost River Range have parallel, kink geometries, are upright to moderately overturned, and plunge shallowly ($<23°$) to either the northwest or southeast (Ross, 1947; Mapel and others, 1965; Janecke and Wilson, 1992; Anastasio and others, 1997). Line length restoration of folds along a 12 kilometers long section in the northern Lost River Range yields a shortening of 2.64 kilometers or 22 percent (Messina, ms, 1993). Most folds within the Lost River Range are décollement folds although fault-bend (for example, Hedlund and others, 1994) and fault-propagation fold geometries (for example, Fisher and Anastasio, 1994) also occur. Depth-to-décollement calculations and results from fold kinematic studies (Anastasio and others, 1997), both suggest a migrating décollement near the base of the McGowan Creek Formation (Antler flysch) (Anastasio and others, 1997). Folds within the upper carbonate section decrease in amplitude eastward as the McGowan Creek Formation thins. Underlying folds in the McGowan Creek Formation decrease in amplitude down section towards the McGowan Creek Formation décollement level. The lower regional décollement for the Hawley creek thrust sheet is in the Precambrian Belt Group and is exposed in the Lemhi Range. The deformation in the Lemhi Range is characterized by large-scale recumbent folding and large-displacement thrusts (Beutner, ms, 1968). Farther east, in the Beaverhead and Tendoy Ranges, basement, thinner Paleozoic section, and synorogenic conglomerates are folded and imbricated within the Cabin, Medicine Lodge, Four Eyes Canyon and Tendoy thrust sheets (Lowell, 1965; Ruppel and Lopez, 1984; Skipp, ms, 1985; Skipp and Link, 1992; Lonn and others, 2000; Harkins and others, 2004a, 2004b).

Subsequent to the Sevier orogeny, the Northern Rockies experienced varying amounts of extension, vertical axis rotation, and tilt as a result of Middle Eocene-Holocene extension on numerous steep and shallow listric extensional faults (for example, Lost River, Lemhi, Pass Creek, and Donkey Hills faults; Crone and Machette, 1984; Janecke and others, 1991; Janecke, 1992; Rodgers and Janecke, 1992; Anders and others, 1993). Many of the extensional faults are confined to range margins and are characterized by carbonate protocataclasities (for example, Pass Creek, Link and others, 1988). However, to the west, a core complex developed exposing more deeply buried lower plate rocks (O'Neil, ms, 1985; Wust and Link, 1988; O'Neil and Pavlis, 1988). Biotite cooling ages ($^{40}Ar/^{39}Ar$ thermochronology; Silverberg, ms, 1990) indicate rapid erosion-controlled or tectonic unroofing of the Pioneer core complex from 48 to 45 Ma and continued ductile deformation in the detachment fault system into the earliest Oligocene. Coeval with extension, much of the region was blanketed by the Challis Volcanics emplaced during two Tertiary magmatic events (45–50 Ma; Janecke and Snee, 1993). Hydrothermal alteration (Criss and Taylor 1983; Criss and others, 1985), Cu mineralization (Criss and others, 1991) and chemical remagnetization (Sherwood, ms, 1994) are associated with this Tertiary magmatic activity.

Lost River Range and Willow Creek Anticline

The Lost River Range is bounded to the west by the seismically active Lost River fault and to the east by the Pahsimeroi basin, which overlaps the range and comprises the hanging wall block of the active Lehmi fault. The northern Lost River Range is a first order synclinorium, which exposes higher order folds such as Willow Creek anticline (figs. 3 and 4). The Willow Creek anticline (Anastasio and others, 1997) is a third order, upright, shallowly northwest plunging, southwest-vergent, asymmetric, décollement anticline. At the level of the Scott Peak Formation, the fold geometry

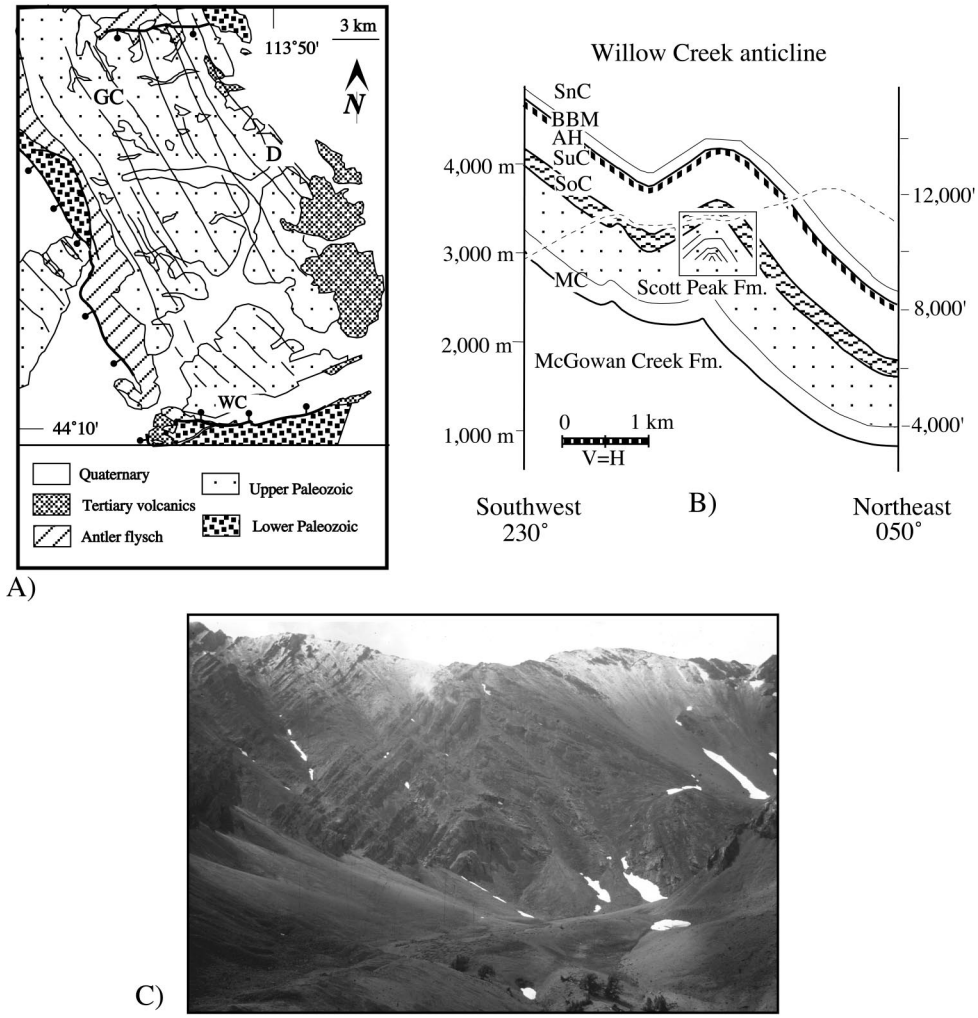

Fig. 4. Willow Creek anticline, northern Lost River Range, Idaho. (A) Simplified geologic map of the northern Lost River Range, Idaho illustrating large-scale synclinorium after Anastasio and others, 1997. (B) Cross section of Willow Creek anticline, inset locates photograph shown in C. (C) Field view of Willow Creek anticline (printed reversed to match section in B) illustrating fold geometry and level of exposure typical of third-order Lost River Range décollement folds.

varies from a close chevron near the core to an open conjugate box shape up-section. Incremental strain histories reconstructed from fibrous overgrowths in strain fringes suggest pinned hinge kinematics during folding (Anastasio and others, 1997). The sense of rotation on opposing limbs indicates that the fiber curvature records primarily the spin of layers through fixed, steep extension directions while the magnitude of the external rotation preserved in the strain fringes is typically less than bedding dip, suggesting a component of layer-parallel shear towards the upper flat panel or pinned hinge during folding.

Our work at Willow Creek anticline was confined to Late Paleozoic carbonates and focused on the Scott Peak Formation, a 625 meter thick limestone unit consisting of interbedded massive biopackstone beds with thinner interbeds of biomicrite. In biopackstone beds, calcite grains are generally <5mm and average 0.63 mm. In

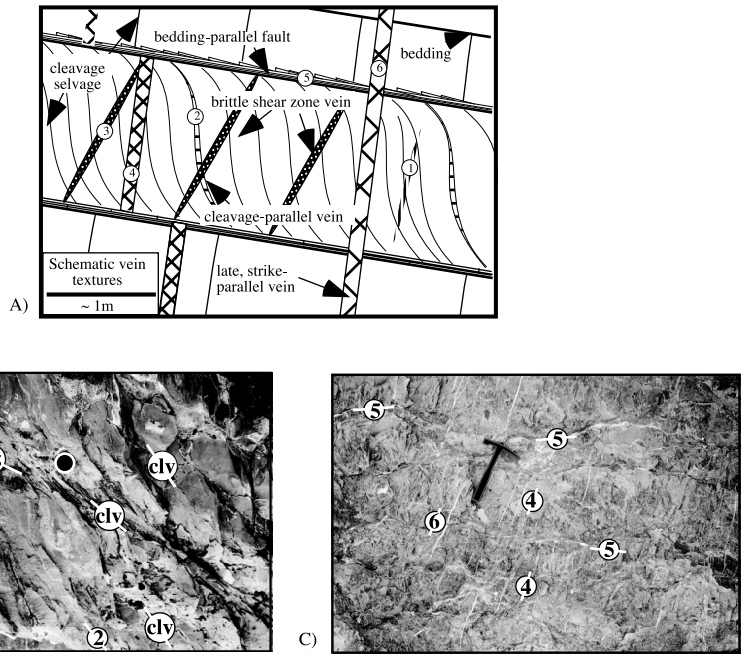

Fig. 5. Mesoscopic structural elements common in the Sevier study corridor. (A) Various vein generations allow a temporal perspective on fluid rock interactions. (B). Field photograph illustrating cleavage geometry in massive layers, deformation zones (dz), and vein generations 1,2 and 5. Lens cap for scale. (C) Field photograph illustrating numerous veins of generations (types) 4, 5 and 6. Rock hammer for scale.

biomicrite layers calcite grains are generally < 1mm and average 0.1mm. Mildly deformed carbonates are composed of 85 to 95 percent calcite, 0 to 10 percent quartz, and <15 percent accessory minerals including goethite, pyrite, anatase, apatite, and <1 percent illite. The massive (>2m thick) biopackstone beds are commonly uncleaved or contain a weak, widely spaced (>10 cm selvage spacing) cleavage. Thinner (<0.25m) biomicrite beds are moderately to strongly cleaved (<2 mm selvage spacing). In general, cleavage forms a divergent fan over the anticline (Anastasio and others, 1997); cleavage is steep in the massive layers and is of variable orientation within the deformation zones. Massive layers dominate the fold and are separated from one another by discrete bedding-parallel faults exhibiting evidence of pressure solution slip, as indicated by calcite shear fibers, or by thin more strongly cleaved bedding-parallel deformation zones, which are often bounded by bedding-parallel faults (fig, 5; Anastasio and others, 1997). Deformation zones compose <5 percent of the overall outcrop volume. Within deformation zones, well-developed cleavage, layer-parallel veins, brittle and brittle-ductile shear zone veins are prevalent. Oriented samples were collected from both massive layers and deformed zones from various structural positions to assess dilation changes accompanying folding and tectonite development. With an objective to study deformation processes, sampling emphasized the more deformed portions of the structure. In addition, calcite veins of various generations and orientations, cleavage selvages, microlithons (less altered zones between cleavage selvages), and undeformed samples were collected and microsampled (1–2mg) for geochemical assessments to explore temporal perspectives on fluid-rock interactions and mass transfer accompanying deformation (fig. 5).

METHODS AND RESULTS

Strain Measurement

To characterize volume changes associated with deformation, finite strains were measured in oriented rock samples collected from various structural positions throughout Willow Creek anticline. Bulk and object finite strains were measured in the cleavage-parallel plane (xy plane, x>y>z principal axes of finite strain ellipsoid) and in the plane perpendicular to the intersection of bedding and cleavage (xz plane) in samples from massive layers and deformed zones throughout the fold (figs. 6 and 7). Cleavage forms a divergent fan across Willow Creek anticline. The poles to planes derived from bedding and cleavage orientations are nearly equivalent (Anastasio and others, 1997) and bedding-cleavage intersections are locally perpendicular to the x-direction determined by straight overgrowths in cleavage-parallel sections. This relationship suggests that cleavage and overgrowth orientations are good macroscopic recorders of the principal strain orientations and that strain ellipsoids can be approximated from two orthogonal ellipse sections.

Bulk finite strain was measured on thin sections using the Fry (Fry, 1979), and enhanced normalized Fry methods (Erslev, 1988; Erslev and Ge, 1990), which evaluates the distribution of framework grain populations. Fry strains were measured on a minimum of 75 carbonate grains over an area of ~1 cm^2. When using the computer program Instrain (Erslev, 1988) object-pair selection factors of between 1.0 and 1.2 were chosen so that analyses included 60 touching pairs for every 100 objects. Object strains, the average (harmonic mean) aspect ratio of elliptical framework grains in a sample, were measured using the R_f/Φ method (Dunnet, 1969) using Earth'nWare Inc. software (DePaor, 1993). In order to test the assumption of an initial random distribution of grains, grain distributions were undeformed and evaluated for uniform distribution (for example, Peach and Lisle, 1979); samples passing a χ^2 test at a 95 percent confidence limit were used in further calculations. Object strains are generally more variable than bulk strains, ranging from R_{xz}=1.5 to 2.4 in deformed zones and 1.0 to 1.6 in massive layers (table 1). Without exception, cleaved layers record greater

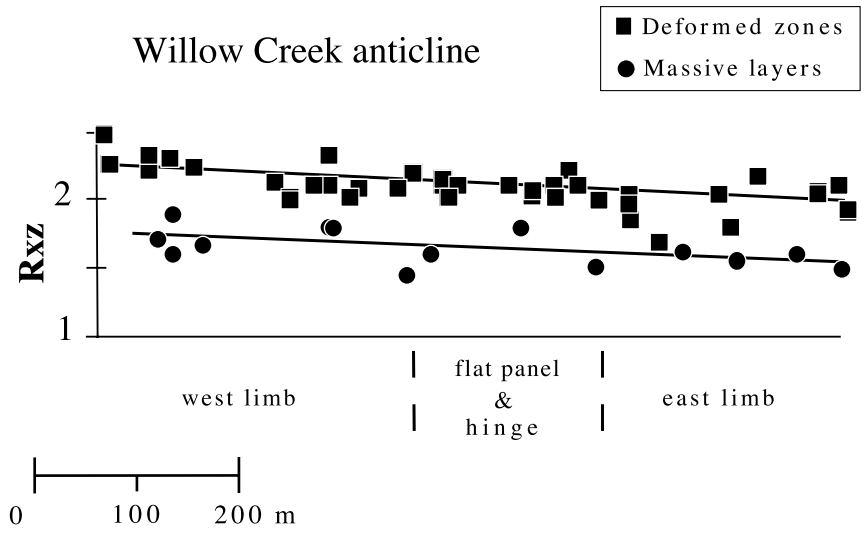

Fig. 6. Finite R_{xz} strain ratio determined by the Fry method (Fry, 1979), as a function of structural and stratigraphic position. Strain is higher in deformation zones than in massive layers and decreases eastward in all layers.

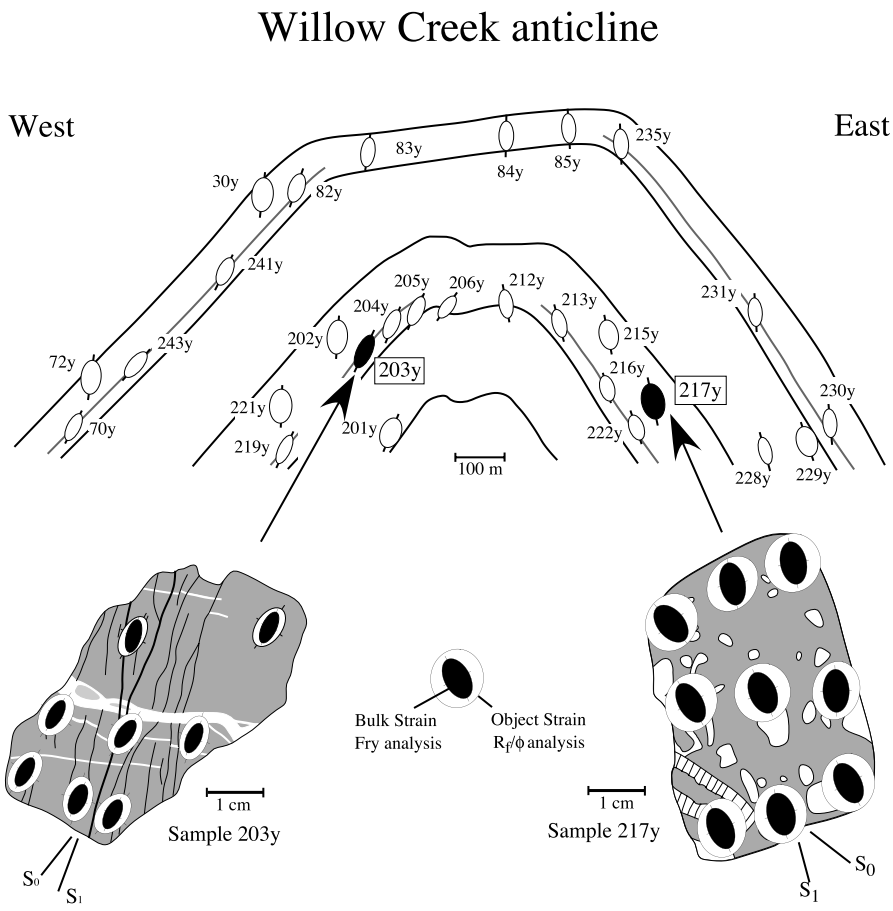

Fig. 7. Sketch of Willow Creek anticline showing sampling sites, sample identification, and measured R_{xz} object strain values and orientations. Finite strain data represents averages of multiple Fry determinations from hand samples. Deformation at the hand sample scale is homogeneous as illustrated for samples 203y from a deformed zone and sample 217y from a massive layer. Strain determinations vary with measurement technique; object strain (R_f/ϕ), outer white ellipse, and bulk strain (Fry) inner black ellipse. In general, strain is homogeneous at the hand-sample scale.

strain magnitude than uncleaved layers from all structural positions. The shorter west-dipping limb exhibited somewhat greater magnitude of strain than the longer east-dipping limb and hinge region (fig. 6).

To test grain-scale strain homogeneity, multiple Fry and R_f/ϕ measurements were made on sample 217y, collected from a massive layer, and 203y, taken from a deformed layer. Multiple strain measurements were made across each sample. In sample 217y object strains were uniformly low with the long axis of the ellipse subparallel to the trace of weak disjunctive cleavage. Bulk R_{xz} strains are nearly constant at ~1.6 across the sample and the long axis of the ellipses are subparallel to the trace of cleavage. In sample 203y, both bulk and object strains are nearly constant across the sample. Bulk strains are ~2.2 to 2.3 while object strains range from ~1.9 to 2.2 over 1 cm^2 areas. The long axes of the ellipses calculated using both techniques are subparallel to the trace of cleavage (fig. 7). In general, each method produced a homogeneous result at handsample scale (~12 cm^2), however, bulk and object strain magnitude and orienta-

TABLE 1

Strain data for Willow Creek anticline samples. Bulk strain determined by Fry analysis (Fry, 1979) using Instrain (Erslev, 1989) and object strain determined by R_f/ϕ method (Dunnet, 1969) using Earth'nWare Inc. software (DePaor, 1993). Plastic strain determined in the xz plane using crinoid axial canal shapes and the R_f/ϕ method. Pressure solution strain determined by direct measurement. See text for further details.

Sample No.	*Srt. Posit.	**Field Class.	R_{xz} Fry	R_{xy} Fry	R_{xz} R_f/ϕ	R_{xy} R_f/ϕ	R_{xz} plastic	e_x plastic	e_x pres. sol.	$1+e_x$ total	$1+e_y$	$1+e_z$	$\bar{e}_s$	ΔV	R_{xy}	R_{yz}
J-200	W	D	1.90	1.30	1.12	1.00	1.30	0.11	0.06	1.17	0.90	0.62	0.46	0.65	1.30	1.46
J-201	W	M	1.60	1.20	1.20	1.04	1.13	0.05	0.10	1.15	0.95	0.72	0.34	0.78	1.20	1.33
J-202	W	D	2.33	1.70	2.30	1.31	1.42	0.16	0.16	1.32	0.77	0.56	0.60	0.57	1.70	1.37
J-203	W	D	2.35		2.30											
J-204	W	D	2.19	1.50	1.60	1.29	1.33	0.12	0.13	1.25	0.84	0.57	0.55	0.60	1.50	1.46
J-205	W	D	2.18	1.54	1.70	1.20	1.42	0.16	0.11	1.27	0.82	0.58	0.55	0.60	1.54	1.42
J-206	H	D	2.15	1.70	2.20	1.40	1.40	0.15	0.16	1.31	0.77	0.61	0.55	0.61	1.70	1.26
J-207	H	D	2.10	1.43	1.69	1.30	1.20	0.07								
J-208	H	D	2.15	1.40	1.67	1.05	1.50	0.18	0.06	1.24	0.89	0.58	0.54	0.64	1.40	1.54
J-210	H	D	1.81	1.41	1.42	1.02	1.25	0.09	0.11	1.20	0.85	0.67	0.42	0.68	1.41	1.28
J-211	H	D	2.05	1.40	1.60	1.30	1.60	0.21	0.08	1.29	0.92	0.63	0.51	0.75	1.40	1.46
J-212	H	D	2.00	1.36	1.35	1.50	1.40	0.15	0.09	1.24	0.91	0.62	0.49	0.70	1.36	1.47
J-213	E	D	2.00	1.30	1.98	1.62	1.12	0.04	0.13	1.17	0.90	0.59	0.49	0.62	1.30	1.54
J-214	E	D	1.90	1.37	1.58		1.21	0.08	0.14	1.22	0.89	0.64	0.45	0.70	1.37	1.39
J-215	E	M	1.60	1.60	1.51	1.23	1.50	0.18								
J-216	E	D	1.79	1.30	1.76	1.22	1.10	0.03	0.15	1.18	0.91	0.66	0.41	0.71	1.30	1.38
J-217	E	M	1.57	1.24	1.04	1.02	1.19	0.07	0.08	1.15	0.93	0.73	0.32	0.78	1.24	1.27
J-218	E	D		1.25	1.57	1.34			0.19							
J-219	W	D	2.48	1.60	1.70	1.28	1.42	0.16	0.13	1.29	0.80	0.52	0.64	0.54	1.60	1.55
J-220	W	D	2.20	1.35	1.92	1.47	1.35	0.13	0.11	1.24	0.92	0.56	0.56	0.64	1.35	1.63
J-221	W	M	1.43													
J-222	E	D	2.17	1.40	1.48	1.18	1.34	0.13	0.17	1.30	0.93	0.60	0.55	0.72	1.40	1.55
J-223	E	D	1.60	1.40	1.10	1.21	1.00	0.00	0.20	1.20	0.86	0.75	0.34	0.77	1.40	1.14
J-228	E	D	2.10	1.34	1.91	1.17	1.18	0.07	0.12	1.19	0.89	0.56	0.53	0.59	1.34	1.57
J-229	E	M	1.50	1.18	1.28	1.35	1.37	0.14								
J-230	E	D	2.03	1.20	1.75	1.15	1.35	0.13	0.10	1.23	1.03	0.61	0.52	0.77	1.20	1.69
J-231	E	D	2.04	1.24	1.92		1.25	0.09	0.07	1.16	0.94	0.57	0.52	0.62	1.24	1.64

TABLE 1
(continued)

Sample No.	*Srt. Posit.	**Field Class.	R_{xz} Fry	R_{xy} Fry	R_{xz} R_f/ϕ	R_{xy} R_f/ϕ	R_{xz} plastic	e_x plastic	e_x pres. sol.	$1+e_x$ total	$1+e_y$	$1+e_z$	$\bar{e}_s$	ΔV	R_{xy}	R_{yz}
J-235	E	D	2.00	1.30	1.80	1.21	1.37	0.14	0.08	1.22	0.94	0.61	0.49	0.70	1.30	1.54
J-237	H	D	2.20	1.40	1.76	1.32	1.25	0.09	0.07	1.16	0.83	0.53	0.56	0.51	1.40	1.57
J-238	H	M	1.60	1.20	1.26		1.03									
J-239	W	M	2.00	1.30	1.45		1.39	0.15								
J-240	W	M	1.80	1.30	1.56		1.51	0.19								
J-241	W	D	2.00	1.20	1.51	1.00	1.17	0.06	0.09	1.15	0.96	0.58	0.51	0.64	1.20	1.67
J-243	W	D	2.22	1.30	1.75	1.21	1.22	0.08	0.07	1.15	0.87	0.52	0.57	0.53	1.30	1.71
S-28	H	M	1.60	1.25	1.65	1.23	1.31	0.12	0.09	1.21	0.97	0.75	0.33	0.88	1.25	1.28
T-30	W	M	1.57													
T-49	H		1.52		1.48											
T-50	H		2.10		1.83											
T-51	H		2.10		2.04											
T-54	W		2.08		1.70											
T-55	W		2.10		1.90											
T-57	W		2.33		2.06											
T-59	W		1.67		1.72											
T-60	W		1.45		1.24											
T-70	W	D	2.25		1.52											
T-72	W	M	1.73		1.70											
T-74	W		2.13		1.61											
T-82	W	D	1.80		1.72											
T-83	H		2.08		1.63											
T-84	H		2.00		2.40											
T-85	H		2.10		1.28											
T-88	H		2.10		2.06											
T-92	E		2.00		1.48											
T-102	E		1.93		2.12											

*Structural Position, W = west limb, H = hinge region, E = east limb. **Field Classification: M = massive bed, D = deformed zone

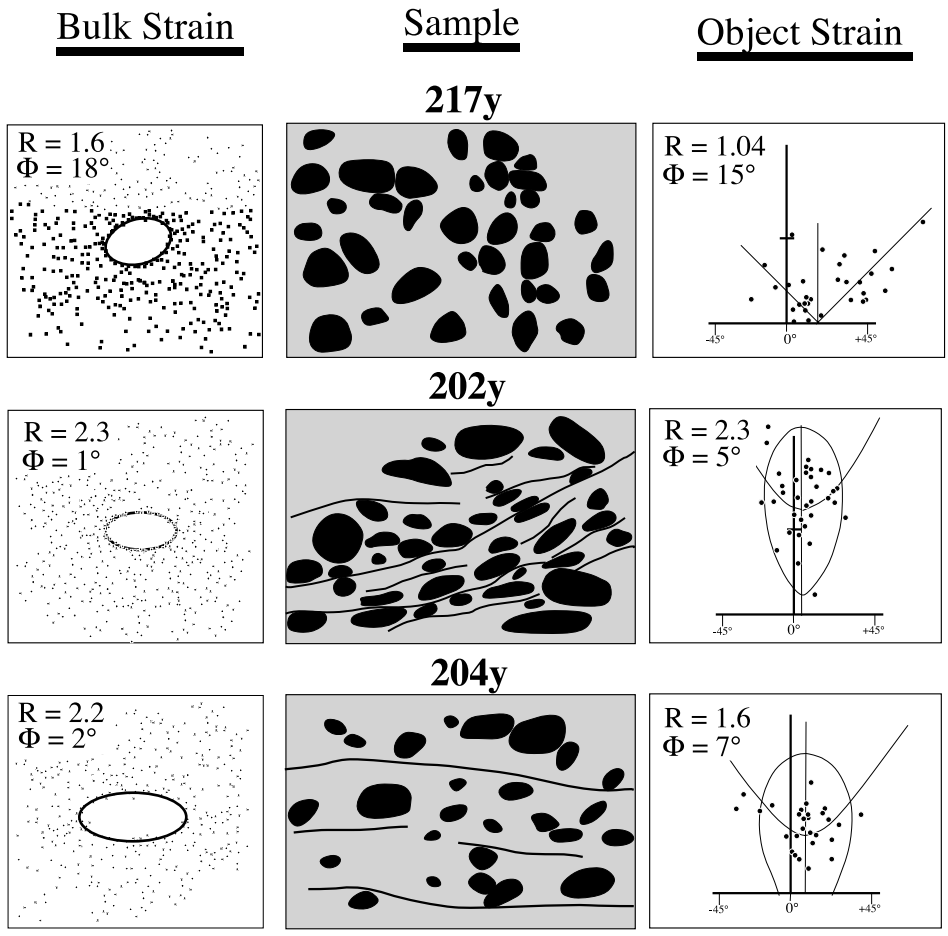

Fig. 8. Comparison of finite strain determination techniques for various sample textures, which are representative of samples from Willow Creek anticline. See figure 7 for sample location. Sample 217y uncleaved biomicrite, sample 202y strongly cleaved biopackstone, and sample 204y, weakly cleaved biomicrite. Bulk strain determined by Fry analysis (Fry, 1979) using Instrain (Erslev, 1989) and object strain determined by R_f/ϕ method (Dunnet, 1969) using Earth'nWare Inc. software (DePaor, 1993).

tion values, varied depending on rock texture (fig. 8). Sample 217y, an uncleaved biomicrite and sample 204y, a weakly cleaved biomicrite, both record greater bulk than object strains, while sample 202y, a strongly cleaved biopackstone, records equivalent bulk and object strains (fig. 9). Comparison of bulk and object strain values in grain supported versus matrix supported rocks suggests that object strain measurements closely match bulk strain measurements in rocks containing <10 percent matrix, however, in biomicrites with >20 percent matrix, bulk strains are 20 to 40 percent greater than measured object strains (fig. 9). Larger calcite framework grains are stronger than the fine-grained micritic matrix and record less strain. Bulk and object strains were measured in the remaining samples at a scale of ~1 cm^2. In the deformed zones, bulk strain ratios (R_{xz}) ranged from 2.0 to 2.5 and averaged ~2.2 on the western limb of the fold. Bulk strain ratios decreased towards the east averaging ~2.0 at the eastern limb of the fold. Average R_{xy} strain ratios are more uniform across the fold ranging from 1.2 to 1.6 and averaging ~1.35. In the massive layers, aspect ratios ranged

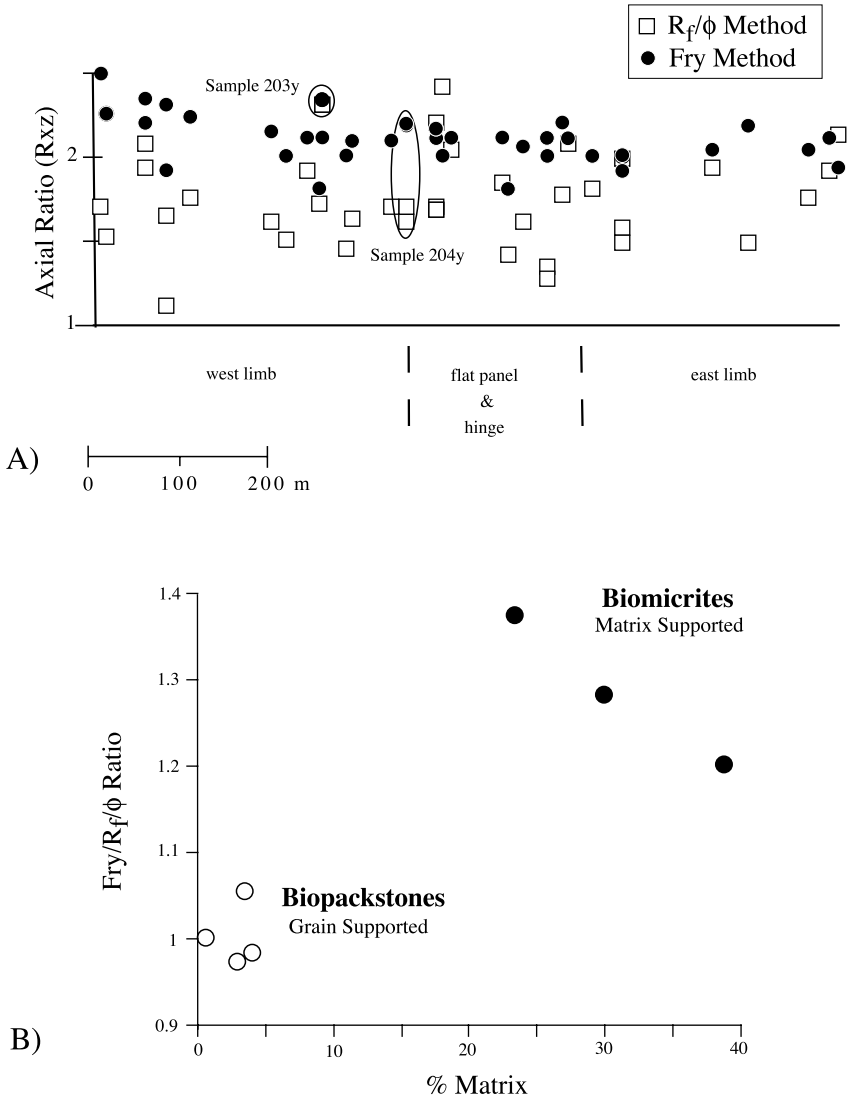

Fig. 9. Summary of the strain data. (A). Corresponding bulk and object strain determinations from representative samples plotted with respect to structural position on the Willow Creek anticline. Bulk strain magnitudes determined using the Fry method and object strains were measured using the R_f/ϕ method on carbonate grains. 203y is a massive layer sample and 204y is a deformed zone sample. (B). Graph of Fry/R_f/ϕ ratio versus % matrix for selected samples. Object strain measured from matrix-supported samples underestimates the bulk sample strain.

from ~1.9 to ~1.6 and averaged ~1.7 at the western edge of the fold. R_{xz} decreases to ~1.5 at the eastern edge of the fold. In massive layers, as in the deformed zones, the principal extension direction (x) is nearly parallel to the trace of cleavage in the fold profile plane (xz plane; orthogonal to fold axis).

Strain Partitioning

In order to use the measured axial ratios to calculate volume strain, it is necessary to calibrate at least one principal strain axis with a direct measurement of extension or

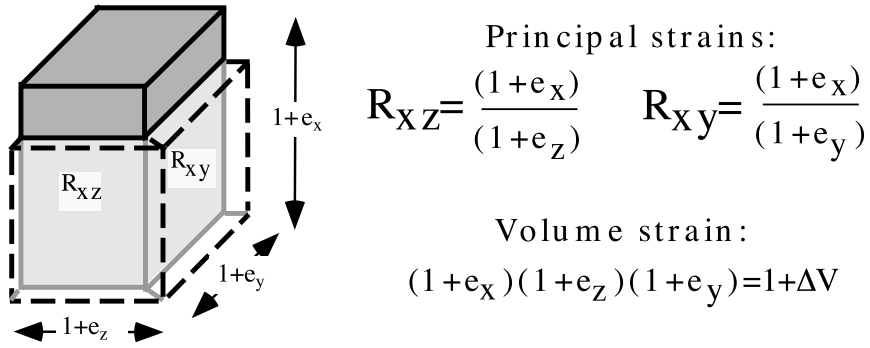

Fig. 10. The method of calculation of volume strain used in this study. Principal strain directions x>y>z. R_{xz}-axial ratio in profile plane and R_{xy}-axial ratio in the cleavage (flattening) plane were determined by Fry analysis, and $1+e_x$, principal extension, measured in the xy plane and partitioned into pressure solution and crystal plastic strain were measured. $1+e_y$-extension in the intermediate principal direction, $1+\Delta V$-dilation, and $1+e_z$-extension in the least principal shortening direction were calculated.

shortening within a homogeneously strained volume (fig. 10). This fact required that length changes associated with the operative deformation mechanisms be quantified. Deformation mechanisms contributing to the overall grain-scale strain at Willow Creek anticline included pressure solution as evidenced by overgrowths and truncated grain boundaries, and crystal plastic strain as evidenced by mechanical twinning, and the rare localized development of deformation lamellae and dynamically recrystallized grains. Pressure solution strains were determined by directly measuring overgrowths and micro-veins, parallel to the trace of cleavage in xz sections and more commonly, parallel to the dip of cleavage and straight fibrous overgrowths in xy sections, in polarized light and cathodoluminescence (at Lehigh on a MAAS ELMS Luminoscope) microscopy. The extension was determined from the average percent of synkinematic calcite in veins and overgrowths recorded in two to three ~2 cm linear traverses in overlapping measurement windows of ~1mm in length across each sample. This approach allowed cm-scale homogeneous domains of extension to be identified in the same thin sections used for R_f/ϕ and Fry analyses where, results are also homogeneous at cm-scales (see fig. 7 and Davidson and others 1998 for further discussion of method). Within the least deformed massive layer samples, principal extension accommodated by pressure solution was <10 percent while extensions within deformed zone samples ranged up to 20 percent (table 1). Extension measurements were consistent across a thin section, however, under recognition of overgrowths in the matrix is possible, which results in an under estimation of the pressure solution strain.

Plastic strains were measured using R_f/ϕ analysis on the axial canal shapes of crinoid ossicles. Undeformed crinoid axial canals are circular in cross section and when deformed, they record only the crystal plastic deformation of the ossicle calcite crystal. Spratt (ms, 1987) showed that crinoid stems are typically short columns or disk-shaped in a study of numerous museum specimens and in stratigraphically equivalent Mississippian carbonates in the southern Canadian Rocky Mountains. Elliptical cross sections resulting from oblique thin section cuts through typical crinoid fossil shapes will be within 24° of the axis of the crinoid stem. This geometry limits the undeformed ellipticity associated with oblique thin section cuts to 1.09 or less, hence

objects suitable for R_f/ϕ analysis. Spratt (ms, 1987) also showed that crinoid stem orientations were uniform in distribution and had originally circular axial canals. Measurement of many grains within each thin section compensates for shape effects due to variable cuts through the ossicles in thin section. Crinoids truncated by thin section cuts were not analyzed (for example, Rowan, 1991). Ellipse shapes were decomposed into principal shortening and extension values assuming twinning produced constant area deformation of the axial canals. Plastic strains ranged from no plastic extension in massive layer samples to 21 percent extension in the most intensely deformed samples (table 1).

The general lack of recrystallized grains and subgrains suggests that dislocation creep was not a significant mechanism of deformation within these rocks and at the low deformation temperatures, grain boundary sliding might be unlikely except as necessary to accommodate other active deformation mechanisms (Mitra, 1976). But Burkhard (1990) showed that grains sliding past each other or other comparable mechanism can produce ductile strains in micritic carbonates even at low temperatures, so our plastic strain values might be minimums at cm-scales. The plastic strains are typically higher in the biosparites, where there is likely little strength difference between framework grains (for example Spratt, ms, 1987), than in the biomicrites where crinoid ossicles are more rigid than the matrix (table 1). The crinoid ossicles could act as stress concentrators, enhancing twinning and thereby overestimating the bulk plastic strain, but we have insufficient data to evaluate these possibilities. Uncertainties associated with the strain measurements come from multiple sources, including thin section cuts which deviate from the principal planes of strain (likely small given low strain ratios), digitizing errors affecting measurements, unrecognized overgrowths, grain boundary sliding, or intragrannular twinning in micrite matrix calcite, or heterogeneous strain partitioning. Based on replicate measurements, we estimate that overall measurement errors are on the order of 10 percent; but the other uncertainties are difficult to quantify.

Using the measurements of plastic strain from crinoids and the extension due to pressure solution recorded by tectonic overgrowths, we calculate the total finite principal stretch for each sample. Measured Fry values of R_{xz} and R_{xy} were then used to determine the intermediate and shortest principal strain values (fig. 10; table 1). Within the massive layers $1+e_x$ averages ~1.15 (15% extension), $1+e_y$ is ~1.0, and $1+e_z$ averages ~0.80 (20% shortening). Within the deformed zones, $1+e_x$ ranges from 1.20 (20% extension) to a maximum of ~1.32 (32% extension) while $1+e_z$ ranges from ~0.7 (30% shortening) to ~0.52 (48% shortening) associated with a very well-developed cleavage. The intermediate axis of finite strain shortens to ~0.80 (20% shortening) in the most deformed samples. To monitor the geometry of strain accumulation, principal stretches were plotted against the amount of strain (Nadai, 1963)

$$\bar{e}_s = 1/\sqrt{3}[(\varepsilon_x - \varepsilon_y)^2 + (\varepsilon_y - \varepsilon_z)^2 + (\varepsilon_z - \varepsilon_x)^2]^{1/2}, \quad (1)$$

$$\varepsilon_{x,y,z} = \ln(1 + e_{x,y,z}), \quad (2)$$

or the stretch on the octahedral planes (45° to the principal directions) of the finite strain ellipsoid (fig. 11). The amount of strain calculated in the least deformed samples was $\bar{e}_s$~0.32. Within deformed zones the amount of strain ranges from $\bar{e}_s$~0.41 in weakly cleaved zones to $\bar{e}_s$~0.64 in strongly cleaved layers. Principal stretches are linear with the amount of strain and trend through a stretch of 1.0 (no finite elongation) suggesting that the suite of samples can be used to approximate the development of the distortion from the least to the most deformed samples. The least and intermediate principal extensions shorten progressively while the greatest direction of extension

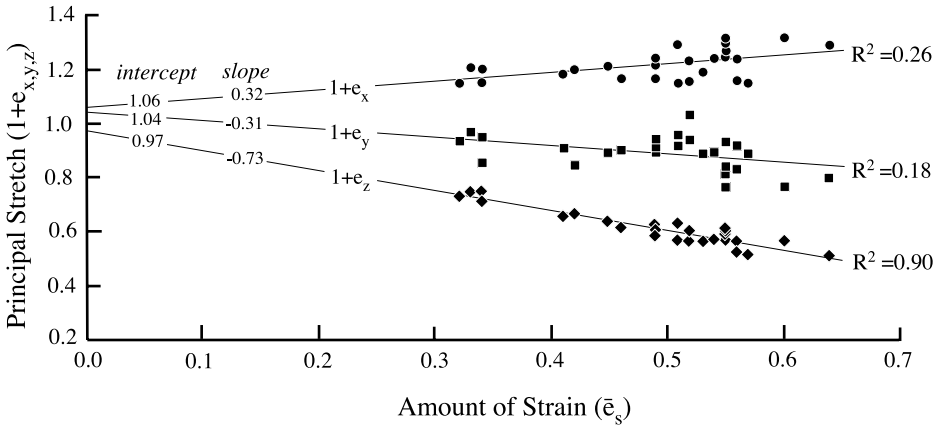

Fig. 11. Principal stretch versus amount of strain (magnitude of strain on the octahedral planes of the strain ellipsoid, Nadai, 1963) for Willow Creek deformed layer samples. Least-square linear regressions of the principal extension data are shown to illustrate the linearity of data and the projection of the extension data through 1.0 (intercepts), which implies that individual data samples a continuous process. Goodness of fit (R^2) shown for illustrative purpose only, plotted variables are not fully independent.

increases as amount of strain increases (fig. 11), similar to the pattern observed by Davidson and others (1998). While there is ample evidence of extension recorded by overgrowths in x and shortening recorded by grain suturing and truncation perpendicular to the z direction, there is only rare textural evidence of suturing perpendicular to y visible in the cleavage planes of Willow Creek anticline. The geometry of the finite strain ellipsoids of the deformed layer samples shows an apparent oblate distortion of nearly all samples, with little correlation between ellipsoid shapes as expressed by Lode's parameter

$$\nu = (2\varepsilon_y - \varepsilon_x - \varepsilon_z)/(\varepsilon_x - \varepsilon_z) \quad (3)$$

and ellipticity (fig. 12). An apparent oblate ellipsoid shape may represent true flattening strain, a combination of compaction and tectonic strain, or plane strain or flattening strain with volume loss (Ramsay and Huber, 1983). Shallow water carbonates, like the Scott Peak Formation likely lithified with shallow burial so significant compactional strains are not expected.

Volume Strain

Local volume changes associated with cleavage development were calculated as the product of the principal stretches

$$1 + \Delta V = (1 + e_x)(1 + e_y)(1 + e_z), \quad (4)$$

where ΔV is the change in volume at the cm^2-scale and are plotted against the amount of strain on figure 13. The data shows a negative linear correlation, with the volume strain decreasing (volume loss increasing) as the amount of strain increases. The correlation line trends towards the origin, suggesting a continuous process of strain accumulation and volume loss. A range of 12 to 22 percent (average ~20%) volume loss was measured within the more massive layers associated with weak cleavage. Within deformed zones, volume strains range from 23 percent volume loss to as much as 49 percent volume loss associated with very well developed cleavage. Also shown on figure 13 are volume strain estimates from Davidson and others (1998), which show similar trends and greater sampling of less strained, lower volume loss samples. In both

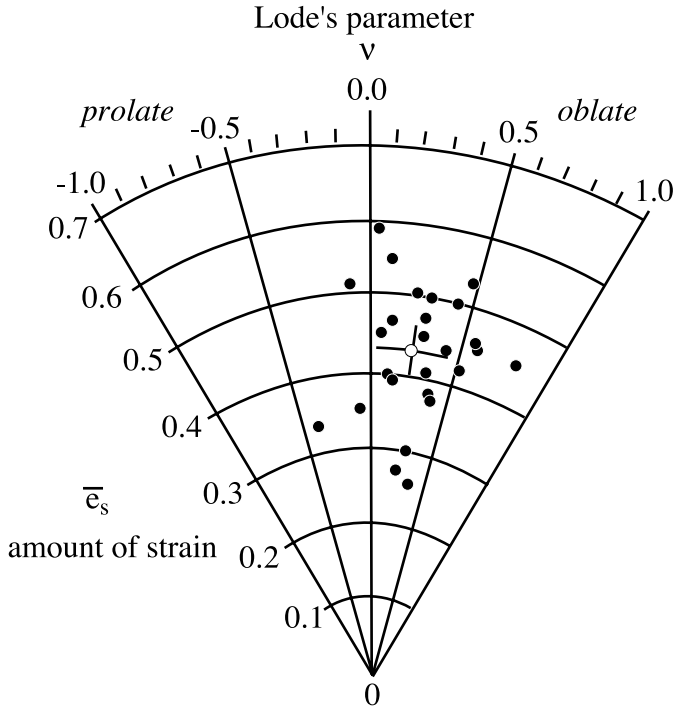

Fig. 12. Plot of Lode's Parameter ν $\{\nu=(2\varepsilon_Y-\varepsilon_X-\varepsilon_Z)\ /\ (\varepsilon_X-\varepsilon_Z)\}$ and amount of strain $\bar{e}_s$ $\{\bar{e}_s=1/\sqrt{3}[(\varepsilon_X-\varepsilon_Y)^2+(\varepsilon_Y-\varepsilon_Z)^2+(\varepsilon_Z-\varepsilon_X)^2]^{1/2}\}$. Open circle-mean strain from all samples showing one standard deviation about the mean. Apparent finite strain ellipsoid is oblate for most samples.

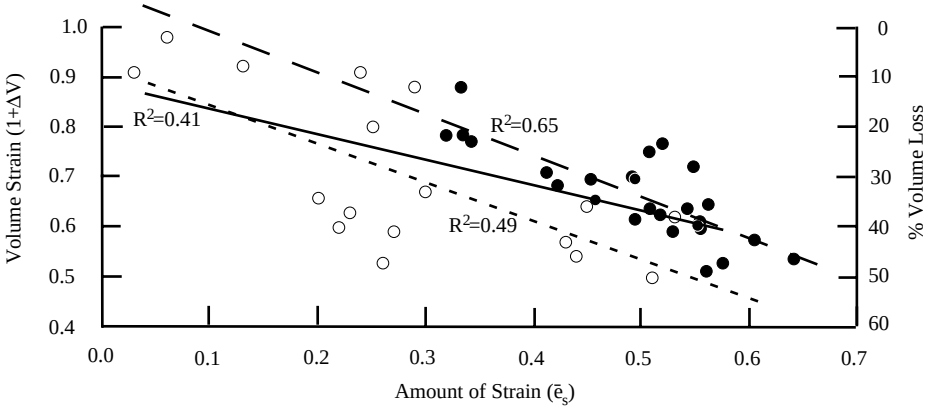

Fig. 13. Graph of dilation [left ordinate: volume strain (1+ΔV), right ordinate: percent (%) volume loss] versus amount of strain for Willow Creek anticline samples. Linear data distribution shown by least-square linear regressions (long dash, data from this study, short dash, data from Davidson and others, 1998, solid line both data sets) suggests increasing volume loss with increasing strain. Goodness of fit (R^2) shown for illustrative purpose only, plotted variables are not fully independent.

studies, which involved the Scott Peak Formation in the Lost River Range, uncertainties in the cm^2-scale volume strain estimates of 10 to 20 percent are likely and are larger for less deformed samples than for more deformed ones (see for example, Davidson and others, 1998).

At smaller scales, dilation is very heterogeneous with large volume gains in overgrowths and veins nearby large losses in selvages and deformation zones. At larger scales, dilation is more difficult to assess. Deformed zones make up a relatively small ($<5\%$) volume of the fold and the massive layers have only modest negative dilations. While veins are prevalent in some portions of the fold, they are conspicuously absent in other areas and overall likely contribute little volume gain at the scale of the entire structure. While it is difficult to quantify dilation at the scale of the entire Willow Creek structure, Davidson and others (1998) showed that both the heterogeneity and the amount of volume strain decreased as the scale of observation increased. For the Doublespring duplex, large volume strains at the cm^3-scale (up to 50%) were insignificant at $100m^3$ to $1km^3$-scales. Given the small volume of highly strained rocks in the Willow Creek anticline, it is likely that large-scale volume loss is comparably small, likely <5 percent.

Geochemistry and Mineralogy

To explore mass transfer accompanying dilation and cleavage formation, major and trace element data were collected for several samples for which strains were determined (table 2). Conventional X-ray fluorescence (XRF) (by X-ray Assay Laboratories Ltd., Don Mills, Ontario, Canada, using standard techniques) was used to characterize major (Na, Si, K, Al, Mg, Ca, P, Ti, and Fe) and trace (Sr) element behavior during cleavage formation in carbonate rocks from the Willow Creek anticline. Sampling for these analyses by microdrilling (sampling at mm to cm scales) was undertaken to preserve the chemical and textural distinctions between microlithons and selvages in the deformed rocks. Chemical data collected from the least deformed massive layer samples are used as a proxy for protolith compositions, and geochemical evolution is established by comparing protolith compositions to compositions of variably strained domains (represented by microlithons and selvages) in the cleaved rocks. Selected major and trace element data are presented in the plots in figures 14 to 16. As expected, as a result of calcite removal during volume loss, CaO and CO_2 (using the loss-on-ignition data as a proxy for CO_2 concentrations) show dramatic correlated decrease in concentration with increasing strain (fig. 14). The trace element Sr also shows depletion (correlated with CaO and CO_2 decrease) with increasing strain (table 2 and figs. 14 and 15B). Other major oxides (TiO_2, Al_2O_3, P_2O_5, MgO, Fe_2O_3, Na_2O, SiO_2, and K_2O) are enriched in selvage areas as compared to microlithon samples, which are in turn, enriched as compared to protolith samples (table 2 and figs. 14 and 16).

To characterize mineralogical changes associated with cleavage development, microsamples from cleavage selvages, microlithons, and massive layers were analyzed using X-ray diffraction (XRD; at Lehigh University on a Philips APD-3720 automated X-ray diffractometer). Samples were first digested in dilute hydrochloric acid to remove any carbonate minerals present. Within the cleavage selvages quartz, illite, kaolinite, quartz, geothite, magnetite, and anatase were present. Scanning electron microscopy (SEM; at Lehigh University on a JEOL 6500F) was used to characterize the texture of microlithons and selvages at a fine scale. SEM observations reveal that neocrystalline clay minerals in selvages are oriented normal to the principal shortening direction, such that their basal planes are parallel to the trace of cleavage in the observed xz sections. Electron dispersive spectrometry (EDS) spectra of microlithons are consistent with XRD analysis indicating an increase in K, Al, and Si concentrations in selvages relative to adjacent microlithons. These increases are associated with

TABLE 2

Major and trace element and oxygen isotope compositions of microsamples. All data are presented as weight % unless otherwise specified

Sample	Sample Texture	$\delta^{18}O$ (V-SMOW)	LOI (used as CO_2)**	Na_2O	MgO	P_2O_5	Al_2O_3	SiO_2	K_2O	CaO	TiO_2	Fe_2O_3	Sr (ppm)	Total
Undeformed (Protolith)														
221A	massive	25.2	38.6	0.05	2.93	0.10	0.30	4.38	0.05	50.9	0.06	0.41	474	97.78
217A	massive	25.2	37.7	0.04	0.65	0.08	0.48	6.18	0.06	50.9	0.06	0.34	578	96.49
217B	massive	25.2	36	0.06	0.72	0.65	0.74	8.97	0.08	50.6	0.07	0.58	518	98.47
229C	massive*	25.5	33.2	0.06	0.52	0.06	1.00	11.8	0.12	47.8	0.10	0.67	515	95.33
229A	massive*	25.5	37.8	0.06	0.57	0.05	0.50	3.94	0.05	54.5	0.07	0.31	527	97.85
Mean (n=5)		25.3	36.66	0.05	1.08	0.188	0.60	7.05	0.07	50.94	0.07	0.46	522	
1σ			2.15	0.01	1.04	0.26	0.27	3.31	0.03	2.38	0.20	0.16	37	
Microlithons														
203C	microlithon	22.3	19.4	0.09	0.52	0.15	1.42	46.4	0.30	28.1	0.10	0.47	270	96.95
229B	microlithon*	25.9	26	0.13	0.77	0.09	2.17	25.0	0.32	40.4	0.15	0.82	366	95.85
202B	microlithon	21.4	14.9	0.08	0.51	0.09	1.44	45.0	0.30	30	0.10	0.76	312	93.18
Mean (n=3)		23.2	20.10	0.10	0.60	0.11	1.68	38.80	0.31	32.83	0.12	0.68	316	
1σ			5.58	0.03	0.15	0.03	0.43	11.97	0.01	6.62	0.03	0.19	48	
Percent mass change relative to Ti (Eq. 8)			**-68.0**	**16.7**	**-67.6**	**-65.9**	**63.3**	**221.0**	**158.3**	**-62.4**	—	**-13.8**	**-64.7**	
Selvages														
202A	selvage	10.6	16.2	0.2	0.73	0.12	3.31	50.6	0.81	23.6	0.22	1.45	231	97.24
203B	selvage	20.9	18.8	0.16	0.84	0.15	3.43	43.6	0.9	26.4	0.22	1.44	227	95.94
Mean (n=2)		15.8	17.50	0.18	0.79	0.14	3.37	47.10	0.86	25.00	0.22	1.45	229	
1σ			1.84	0.03	0.08	0.02	0.08	4.95	0.06	1.98	0.00	0.01	3	
Percent mass change relative to Ti (Eq. 8)			**-84.8**	**14.6**	**-76.7**	**-76.3**	**78.7**	**112.6**	**290.9**	**-84.4**	—	**0.3**	**-86**	

*Sample 229y contains a massive part (on right in fig. 17c) and relatively deformed part (on left in fig. 17c). No selvage material was obtained for this sample, as selvages are quite narrow.

**LOI data are used to represent the CO_2 content of these samples, but the H_2O content of clay minerals in the microlithons and selvages also contributes somewhat to large volatile contents.

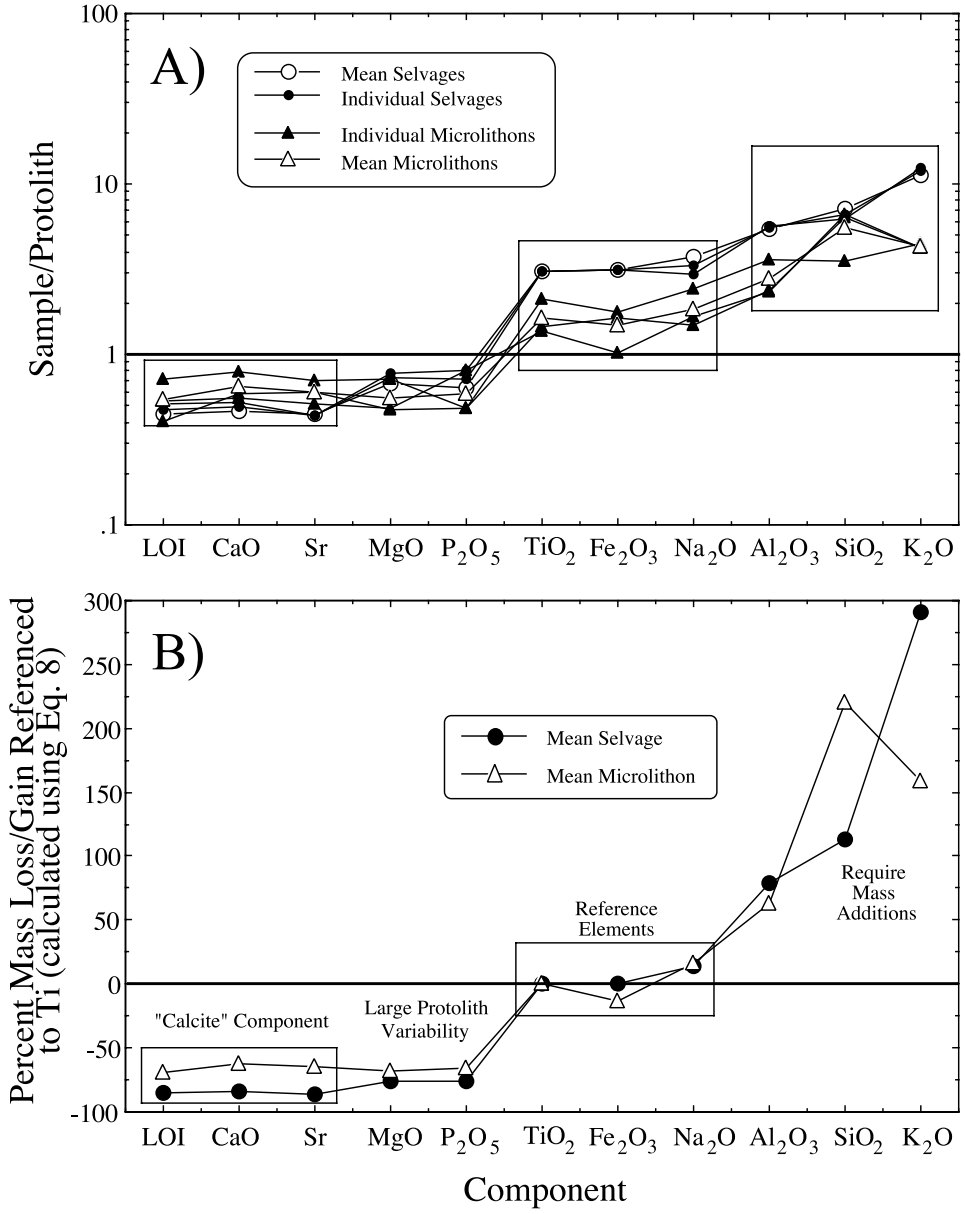

Fig. 14. (A) Plot of ratios of sample oxide/element concentrations in microlithons and selvages (and mean microlithon and selvage concentrations) to concentrations of the same oxides/elements in the protolith. Oxides/elements for which ratios are <1 are inferred to have been lost during volume strain, and those with ratios >1 are those which are either thought to have been passively concentrated during volume loss (CaO, LOI, Sr) or enriched by additions by infiltrating fluids (Al_2O_3, SiO2, and K_2O). (B) Plot of mass gains and losses calculated using equation 8, based on use of Ti as the immobile reference element. Note that CaO, LOI, and Sr were uniformly removed during volume loss, whereas Al_2O_3, SiO2, and K_2O (possibly also Na_2O) appear to have been added to the microlithons and selvages during the deformation. Greater variability in the protolith compositions (see table 2) obscures the behavior of MgO and P_2O_5 in these rocks.

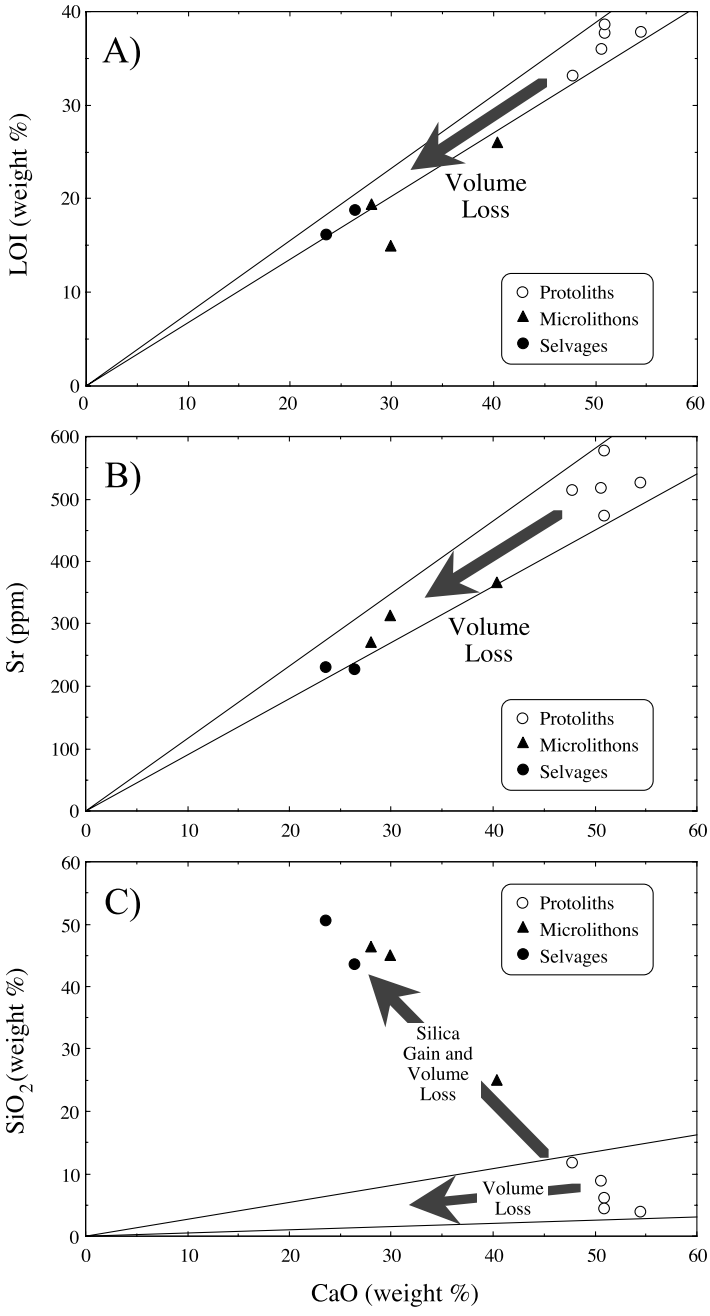

Fig. 15. Plots of element/oxide concentrations (LOI, representing CO_2, Sr, and SiO_2, the latter included to demonstrate its contrasting behavior) versus CaO concentrations in protolith carbonates, microlithons, and selvages. CaO, LOI, and Sr depletions in the deformed lithologies (with the selvages showing the greatest depletion) relative to protoliths are consistent with removal during volume loss related to removal of a "calcite component" (see arrows on A and B), whereas SiO_2 enrichments accompanying CaO removal are best explained by Si additions during volume loss (see arrow on C).

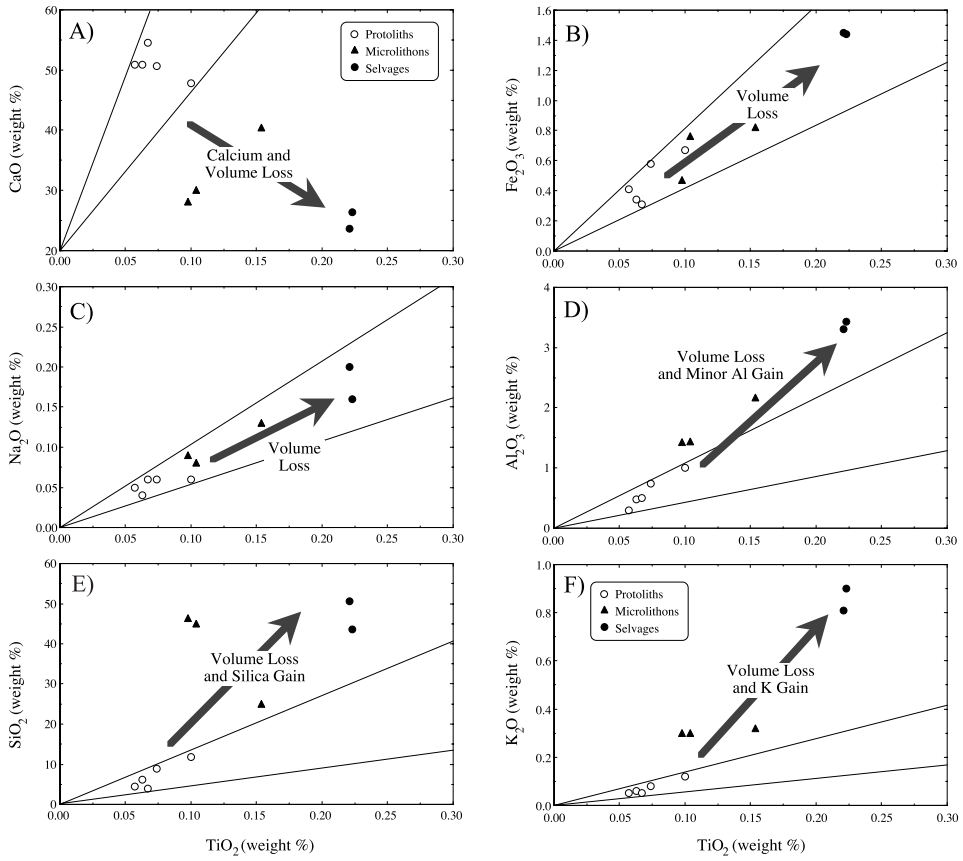

Fig. 16. Plots of element/oxide concentrations (Fe_2O_3, Na_2O, Al_2O_3, SiO_2, K_2O, and CaO, the latter for which a plot is included to demonstrate its contrasting behavior) versus reference TiO_2 concentrations in protolith carbonates, microlithons, and selvages. The plots of Fe_2O_3 and Na_2O versus TiO_2 are better explained by passive concentration during volume loss (see the arrows in B and C; cf. Ague, 1994; Yonkee and others, 2003), whereas the variations in Al_2O_3, SiO_2, and K_2O concentrations with TiO_2 concentration appear to require significant Al-Si-K additions during volume loss (D-F; again, see Ague, 1994; Yonkee and others, 2003). In (A), a plot of CaO concentrations versus TiO_2 is provided to illustrate the very different behavior of CaO (see the shaded arrow indicating a trajectory of CaO loss during volume loss).

increased abundances of illite and kaolinite in selvages (2:1 illite to kaolinite ratio) identified using combined XRD/XRF analysis.

Stable Isotope Data

Carbon and oxygen isotope analyses were undertaken to explore the scale at which the thrust belt behaved as an open system during deformation. Samples were collected from massive layers, deformed zones, and several generations and types of veins at Willow Creek anticline and as done at other localities transecting the Montana recess (see Davidson and others, 1998; Bebout and others, 2001; Johnson, ms, 2002; A. Johnson, D. Anastasio, and G. Bebout, manuscript in preparation). Carbon dioxide was liberated from calcite using H_3PO_4 following the method of McCrea (1950) and samples were analyzed using the Finnigan MAT 252 mass spectrometer at Lehigh University. Data are presented in standard notation (in ‰), according to:

$$\delta^{18}O = 1000[\{(^{18}O/^{16}O)_{Sample}/(^{18}O/^{16}O)_{Standard}\} - 1] \quad (5)$$

and

$$\delta^{13}C = 1000[\{(^{13}C/^{12}C)_{Sample}/(^{13}C/^{12}C)_{Standard}\} - 1]. \quad (6)$$

Oxygen and carbon isotope values are reported relative to Vienna Standard Mean Ocean Water (V-SMOW) and Pee Dee Belemnite (PDB), respectively. Proper standardization for the O- and C-isotope analyses was verified by analysis of various laboratory and international carbonate standards including NBS-19 (calcite). For ~145 analyses of one internal calcite standard (sample 8-3-7v, calcite vein), over a nine year period, uncertainties (expressed as 1σ) are 0.15 permil and 0.10 permil for $\delta^{18}O$ and $\delta^{13}C$, respectively.

At Willow Creek anticline, the $\delta^{18}O$ of calcite in whole-rock samples collected from the least deformed layers averages ~+25 permil, whereas whole-rock samples from deformed zones are generally lower in $\delta^{18}O$ than less deformed samples, with the whole-rock values for deformed zones ranging from +22 to +24 permil (fig. 17A). Veins show an extremely wide range of $\delta^{18}O$ (figs. 17 and 18), and multi-generational vein complexes, which contain multiple generations of massive or fibrous calcite, show significant across-vein variations in $\delta^{18}O$, ranging from +6 to +27 permil (see figs. 17A and 18).

To explore spatial heterogeneities of open- or closed-system behavior, microsamples were collected from cleavage selvages, microlithons, and veins by microdrilling and analyzed for their C and O isotope compositions (fig. 17B–E). Large differences in $\delta^{18}O$ exist between adjacent microlithons, veins, and selvage domains (fig. 17 C, D, and E). Mildly deformed samples such as 229y have relatively uniform stable isotopic compositions with calcite $\delta^{18}O$ ranging between +25 and +26 permil, similar to protolith values, but with one vein having significantly lower $\delta^{18}O$. In contrast, calcite $\delta^{18}O$ values measured in microsamples of selvages in more deformed samples, such as samples 202y and 203y, range from +11 to +21 permil and are generally lower in thicker, better developed selvage zones (for example, thicker line on fig. 17E). Microlithons have calcite $\delta^{18}O$ values lower than those of massive undeformed whole-rock samples, with values for microlithons mostly ranging from +21 to +23 permil (near +25‰ for the undeformed whole-rock samples). Veins (bulk/whole-rock and microsamples) exhibit a broad range in calcite $\delta^{18}O$ values (+6 to +26‰), with large inter- and intravein variation (figs. 17 and 18). Some veins of all generations other than Type 3 (see fig. 5) have $\delta^{18}O$ values leveling off in the range of +5 to +10 permil similar to what Davidson and others (1998) observed at the Doublesprings duplex (also in the Lost River Range). However, for the later-stage veins, particularly Types 4 and 6, nearly all samples are extremely low in $\delta^{18}O$ (fig. 18). Data for the several individual microdrilled samples together exhibit a range in stable isotopic values equivalent to the range recorded by the entire suite of whole-rock samples (see similarities in fig. 17A and 17B). The $\delta^{13}C$ values for microsamples show little variation among microlithons and veins, which together range from –0.3 permil to +2.3 permil, as compared to selvage samples which range widely from –5.8 permil to +2.4 permil (fig. 17B).

DISCUSSION

Mechanisms of Cleavage Development

Strain geometry.—Observations at Willow Creek anticline demonstrate a high degree of strain heterogeneity at 10^{-3} m to 10^{1} m scale. At a scale of 10^{-2}m (a few centimeters), homogeneous domains of both relative axial ratios (R_{xz}, R_{xy}) and principal extensions ($1+e_x$) were established. Therefore, it is only at the scale of a few centimeters that our calculations of volumetric distortion are valid. Anisotropic volume loss affects the shape of the finite strain ellipsoid (Ramsay and Wood, 1973;

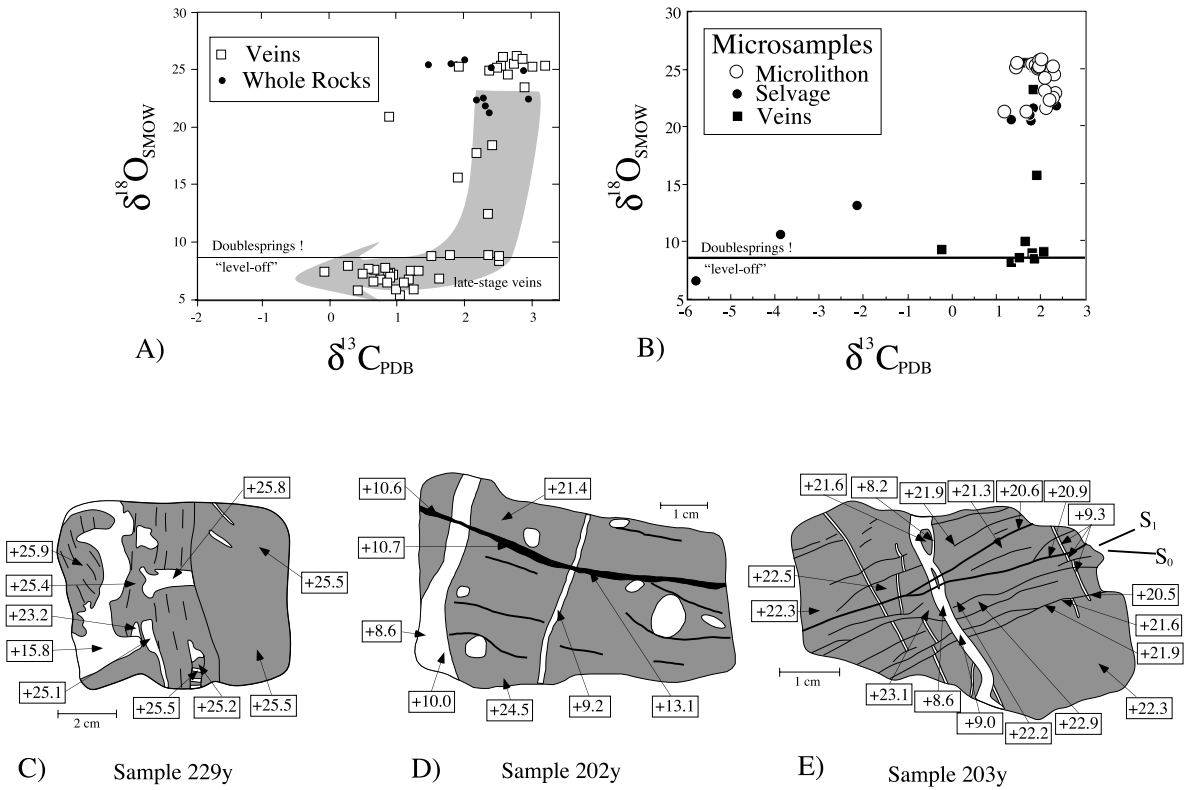

Fig. 17. Stable isotope data. (A) Plot of $\delta^{18}O_{V\text{-}SMOW}$ versus $\delta^{13}C_{PDB}$ for Willow Creek veins and whole rock samples. Also shown is the position of the Doublesprings duplex vein "level-off" in $\delta^{18}O$ (Davidson and others, 1998). (B) Plot of $\delta^{18}O$ versus $\delta^{13}C$ for Willow Creek microsamples of microlithon, cleavage selvage and vein samples from deformation zones. The position of the Doublesprings duplex vein "level-off" (Davidson and others, 1998) is also shown. (C) Hand sample sketch and $\delta^{18}O$ values obtained by microdrilling sample 229y, from a massive layer. (D) Hand sample sketch and $\delta^{18}O$ obtained by microdrilling sample 202y, a cleaved biosparite. (E) Hand sample sketch and $\delta^{18}O$ values obtained by microdrilling for sample 203y, highly cleaved biomicrite. All show small-scale heterogeneity in fluid-rock interaction based on isotope compositions.

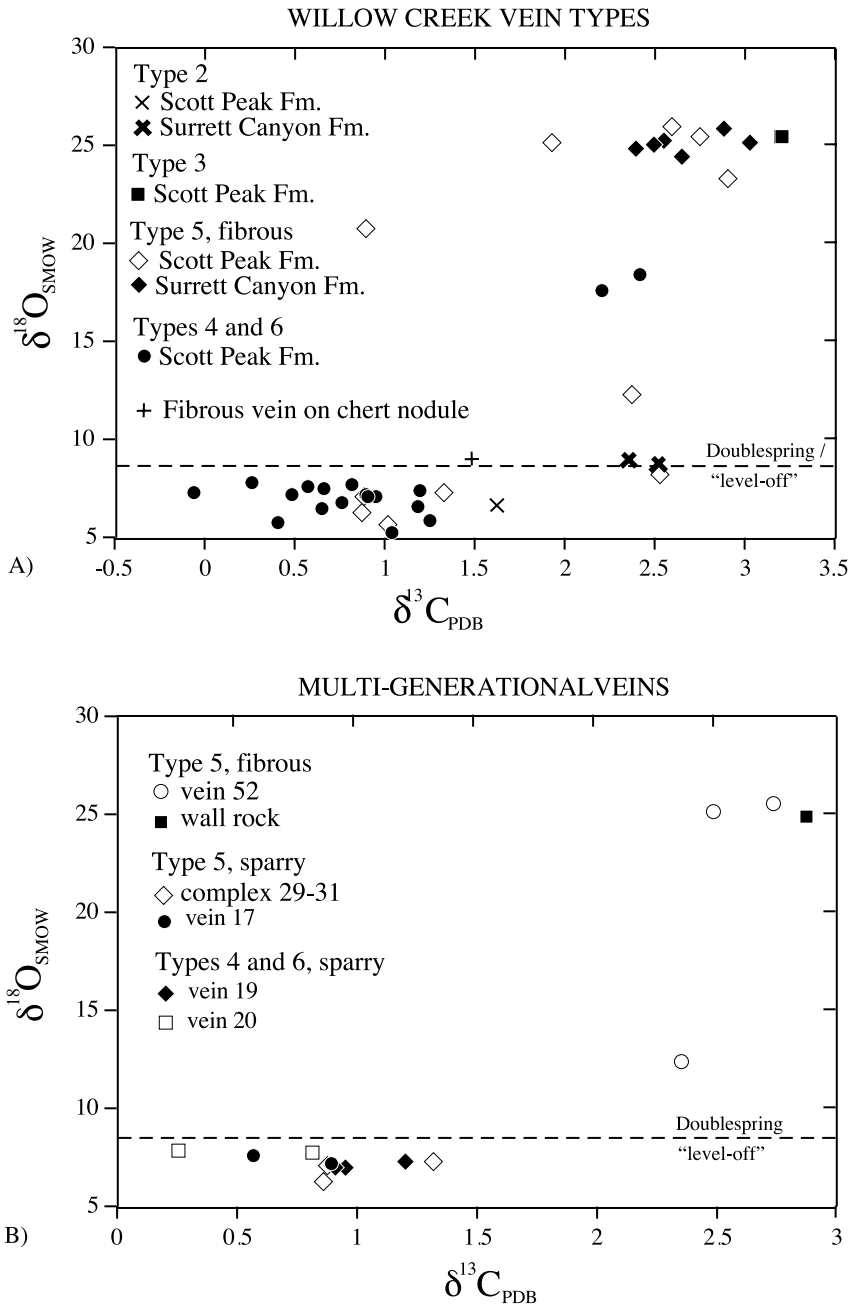

Fig. 18. Stable isotope plot of vein microsamples from single generation veins of varying type (A) and multi-generational veins (B). In both (A) and (B), the position of the Doublesprings duplex vein "level-off" in $\delta^{18}O$ (Davidson and others, 1998) is also shown. For both plots, vein types are distinguished using the labeling introduced in fig. 5. In (A), veins are also broken down by formation (Scott Peak and Surrett Canyon Formations). Vein types 4-6 are regarded as having formed contemporaneously and during folding.

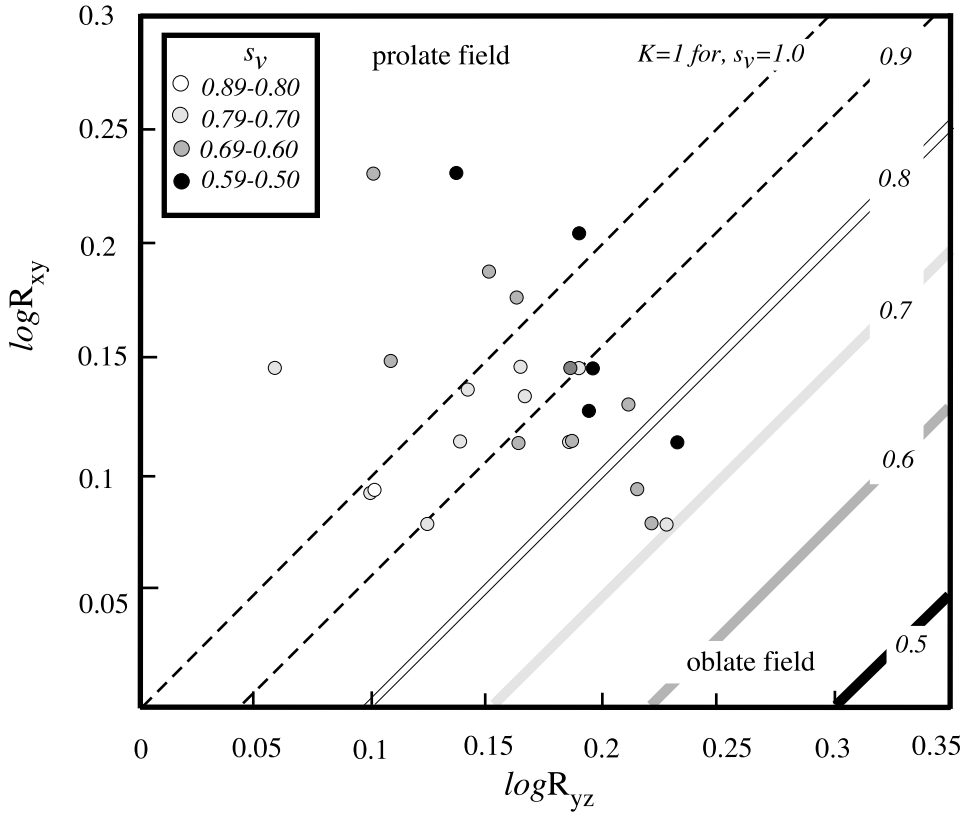

Fig. 19. Logarithmic Flinn diagram for Willow Creek samples. This graphical representation of the shape of an ellipsoid is generated by plotting log R_{yz} as abscissa and log R_{xy} as ordinate. Plane strain lines (K=1) for varying amounts of volume strain (0.9-0.5) are also shown. Graph illustrates prolate nature of strain when ellipsoid shape as well as volume strain is considered.

Ramsay and Huber, 1983). The linear increase in principal extension observed in the Willow Creek samples does not balance the combined shortening observed in the intermediate and shortening directions at a thin section scale (fig. 11). Figure 19 plots ellipsoid shapes on a logarithmic Flinn graph (Ramsay, 1967), contoured for plane strain with a range of negative dilations. Comparison of ellipsoid shapes and volume strains indicates that finite strains are actually prolate (two principal directions shortened, one lengthened) rather than oblate (one principal direction shortened, and two extended), as many samples appear when dilatancy is neglected (fig. 12). Cleavage intensity correlates with the amount of strain and amount of volume loss, with well-cleaved rocks recording greater volume loss than rocks with weak or no macroscopic cleavage.

Geochemical approach.—An examination of figures 14–16, and some simple calculations of mass loss and gain, allow the elements for which data are presented in table 2 to be assigned to one of several categories of behavior during the cleavage formation. In figure 14, concentrations of each element or oxide in the microlithons and selvages are compared with concentrations in the presumed protolith (table 2), showing data for both individual samples and mean microlithons and selvages. On figure 14A, it is evident that, whereas some elements (CO_2, here represented by the LOI data, CaO, MgO, and Sr; note the larger uncertainty in the protolith concentrations for MgO and

P_2O_5 in table 2) are fairly uniformly depleted in microlithons and selvages relative to protoliths (that is, with their sample/protolith ratios plotting significantly <1 on this figure), others are enriched to varying degrees (that is, have sample/protolith ratios significantly >1). Some oxides (TiO_2, Fe_2O_3, and Na_2O) are present in microlithons and selvages at ~1.5-3x the protolith concentrations, and a third group of oxides (Al_2O_3, SiO_2, and K_2O) shows enrichments of 3-11x in the microlithons and selvages relative to those in the protolith. TiO_2 and Fe_2O_3, and possibly also Na_2O, show enrichments of ~50 to 20 percent in microlithons and selvages most consistent with passive enrichment during the removal of a significant fraction of the rock mass in carbonate indicated by the data for CaO, CO_2, and Sr (table 2). Because of this relationship and the common consideration of Ti as a relatively immobile "reference element" in considerations of mass and volume change (see for example Ague, 1994; Yonkee and others, 2003), we adopt Ti as a reference element in further discussions (the calculations presented in fig. 14B are discussed below). Figure 15 demonstrates that the co-variations of CaO, CO_2, and Sr (expected to reside largely in calcite in rocks such as these) are consistent with their simultaneous loss during removal of a "calcite" component (fig. 15A and 15B), whereas SiO_2 concentrations appear to be affected by significant mass gain not attributable to the "calcite" component mass loss (see plot of CaO vs. SiO_2 in fig. 15C). In figure 16, we plot the remaining oxides (including SiO_2) against TiO_2 concentrations as a means of illustrating their behavior relative to this reference element during the deformation (see use of similar plots by Ague, 1991, 1994; Yonkee and others, 2003). On these plots, it is evident that a number of components, particularly Al_2O_3, SiO_2, and K_2O, were added to the rocks during the formation of cleavage (see the trends on these plots expected as the result of volume strain and element gain; see for example Ague, 1994; Yonkee and others, 2003).

A commonly employed approach toward calculating mass and volume change during deformation and metasomatism involves comparison of element concentrations of variably deformed rock samples to concentrations of reference species such as Al or Ti, which are regarded as being relatively immobile (Ague, 1991, 1994; Erslev and Ward, 1994; Goldstein and others, 1995; Yonkee and others, 2003). Based on our assessment above that Ti (and perhaps also Fe and Na) concentrations in microlithons and selvages best approximate those expected as the result of the volume loss reflected by the Ca, CO_2, and Sr decreases in the same samples (table 2 and figs. 14–16), we calculate the total change in mass using Ti concentrations for reference as:

$$\%\ \text{change in mass} = [(C_i^o/C_i') - 1] \times 100 \qquad (7)$$

where C_i^o and C_i' are the concentrations of i (immobile reference species) in the initial and final states, respectively (Ague, 1991, 1994). Comparisons of the compositions of the two textural domains (microlithons and selvages) in more deformed samples to the protolith composition yields estimated mass change (loss in this case) of −42 percent from protolith to microlithon, and −68 percent from protolith to selvage, again, using Ti as the reference species. We use the following equation to calculate the mass change of the other oxides and Sr relative to Ti (see table 2):

$$\%\ \text{mass change of species j} = [(C_i^o/C_i') \times (C_j'/C_j^o) - 1] \times 100 \qquad (8)$$

where C_i^o and C_j' are the concentrations of j (mobile species) in the initial and final states, respectively (Ague, 1991, 1994). Comparison of protolith and microlithon compositions suggests significant loss of Ca, CO_2, Mg, and Sr (possibly also P) and addition of Si, Al, and K (table 2; fig. 14B). Note that, using the Ti reference frame, Al_2O_3 mass changes of +63 percent and +79 percent are calculated for microlithons and selvages, respectively, arguing against any assumption of coherent Al-Ti conserva-

tive/immobile behavior for these rocks (also see the differing apparent enrichments of Ti and Al indicated by the plots in fig. 14).

Again, using Ti as the immobile element reference frame, the volumetric strain associated with cleavage development can be estimated by:

$$\Delta V = [(C_i^o/C_i') \times (\rho_o/\rho') - 1] \times 100, \quad (9)$$

where ρ_o and ρ' are the initial and final rock densities (Ague, 1991, 1994). Assuming no density change during deformation, dilation recorded geochemically in microlithons are the same as the total mass losses (eq 7), calculated at 42 percent, using Ti as the reference element. Dilation estimated from the selvage geochemistry is −68 percent, again referenced to Ti concentrations changes. As was discussed in more detail by Davidson and others (1998), using both geometric approaches to estimating volume strain and a larger geochemical dataset including data for whole-rocks, the discrepancy between the dilation predicted geochemically and that measured by the volumetric distortion through geometric methods can be attributed to small-scale chemical heterogeneity between microlithons and selvages. The larger-scale strain measurements based on geometry and average microlithon and selvage distortions, result in lower estimates of volume loss (for this study, up to ~50%) relative to the volume loss estimated from the geochemistry of the mm-scale selvages (nearly 70% volume loss for the mean selvage composition; see for example Davidson and others, 1998).

Authigenic illite and kaolinite are abundant in selvage domains and are the presumed repositories for components enriched in these domains (particularly Al_2O_3, SiO_2, and K_2O; presumably also H_2O and other trace elements which commonly reside in clay minerals that were not analyzed in our study), and the enrichments point to open-system behavior at least at the scales examined. The deformation mechanism of pressure solution is enhanced with increasing phyllosilicates content as phyllosilicate-carbonate grain boundaries serve as fluid pathways (Marshak and Engelder, 1985). Growth of phyllosilicate phases during deformation would enhance the pressure solution strain rate and enhance fluid advection in selvages, generating positive feedback between strain and metasomatism (for example, Davidson and others, 1998). Loss of calcite accompanying oriented clay growth would result in chemical and geometric strain softening in the deformed zones, enhancing the feedback mechanism. The varying degrees of element enrichment, corresponding to varying extents of progressive deformation in microlithons and selvages, reflect a continuum in the extents of coupled deformation, fluid-rock interaction, and related mass transfer (also see Davidson and others, 1998). It is worth noting that, whereas microdrilling at scales of a few mm^3 demonstrates the distinctive element compositions of various textural domains (figs. 14–16), it likely still results in the sampling of even finer-scaled nascent selvages within microlithons that have been observed by SEM methods.

Fluid Sources and Driving Mechanisms

The geochemical data presented here have implications for the paleohydrology of the Sevier orogen. Both the major and trace element and the stable isotope data require some open-system behavior to accommodate tectonite development during folding of the Willow Creek anticline. Because of our focus on fluid-rock interactions associated with deformation and the similarity in vein and microlithon C-isotope values (figs. 17 and 18), we focus this discussion on O-isotope systematics (also see Bebout and others, 2001). Whole rock and microlithon samples have calcite $\delta^{18}O$ values of ~+25 permil, characteristic of marine carbonates, whereas, microsampled selvages and many veins have values more than 15 permil lighter (figs. 17 and 18). The large shift in $\delta^{18}O$ is incompatible with closed-system behavior, however, it is consistent with infiltration of deformation zones and fractures by externally-derived, isotopically

lighter fluids. We interpret the large variation in $\delta^{18}O$ in selvages and veins as a reflection of variable up-stream fluid-rock isotopic exchange histories. The large, shaded arrow on fig. 17A demonstrates a generalized exchange trajectory involving a C-poor, O-rich (likely aqueous in this case) fluid with relatively low $\delta^{18}O$ and $\delta^{13}C$ (see the calculations by Rye and Bradbury, 1988). While some early fibrous veins and strain shadows contain calcite with near protolith $\delta^{18}O$ values, the latest-stage veins at Willow Creek anticline have $\delta^{18}O$ values which level-off in the range of +5 to +10 permil. We have found similar patterns in O-isotopic heterogeneity in deformed carbonates throughout the Montana recess (see Davidson and others, 1998; Bebout and others, 2001). The latest-stage veins are more likely to record the later-stage fluid flow, which was dominantly discontinuity based (faults, fractures). Fluids infiltrating along discontinuities are better able to retain the isotopic composition of their sources, as they likely experienced increased fluid fluxes, limiting up-stream alteration as a result of fluid-rock exchange. Comparison with the O-isotopic signature of fibrous overgrowths and veins suggests that early, closed system, porosity-based permeability with dispersed, intergranular flow, evolved into a discontinuity-based, open system permeability, with focused fluid flow, as a result of strain localization; similar to deformation enhanced permeability evolution interpreted elsewhere (for example, Rye and Bradbury, 1988; Caine and others, 1996; Davidson and others, 1998). In carbonates (low-porosity, low permeability, monomineralic, polycrystalline aggregates), positive dilation of faults, and fractures during episodic fluid pressure increases likely enhanced focused fluid flow permeability by >2 orders of magnitude (Carson and Screaton, 1998).

We have previously shown (Davidson and others, 1998; Bebout and others, 2001), and have also demonstrated here, that pervasive fluid infiltration is heterogeneous at small scales and intimately associated with fabrics related to compressional faults and fault-related folds. Therefore, we attribute the isotopic alteration of Willow Creek carbonates to Sevier orogenesis, rather than to the Tertiary magmatism or Basin and Range extension, which has also affected the study corridor. Furthermore, there would have been an inadequate supply of exsolved magmatic fluids to generate the observed metasomatism at a regional-scale and the $\delta^{18}O$ values calculated for the waters that infiltrated the thrust belt are inconsistent with a magmatic source (for example, ~5.5‰ to +10‰, Sheppard and others, 1969; up to +20‰, Nesbitt and Muehlenbachs, 1991). They are also lower than those expected for devolatilized fluids equilibrated at higher temperatures at greater depths in the thrust belt (for example, > +10‰, Evans and Battles, 1999), which migrate in response to thrust loading (squeegee mechanism, Oliver, 1986; Machel and others, 2002). Such fluids, although likely generated during orogenesis, were likely stratigraphically isolated from the upper thrust wedge by the Antler flysch (McGowan Creek Formation), an aquitard, which extends across the entire study corridor. Using the minimum range of calcite $\delta^{18}O$ values (+5 to +10‰) and employing calcite-H_2O fractionation factors from O'Neil and others (1969) for the estimated temperatures of deformation (150° to 250°C), the calculated $\delta^{18}O$ values for H_2O range from -7.5 to +2.5 permil. These $\delta^{18}O$ values of late-stage veins and deformed zone samples are consistent with infiltration and exchange with near shore meteoric water with seawater-like O-isotope composition (for example, $\delta^{18}O$ of 0‰ to –5‰, Kendall and others, 1995). We interpret $\delta^{18}O$ values of earlier-formed veins and the microlithons within deformed zones to reflect varying degrees of exchange of these meteoric fluids with high $\delta^{18}O$ carbonates and varying local fluid-rock ratios.

A likely source of the meteoric fluids impacting the Sevier orogenic foreland was the nearby Western Interior Seaway, whose western shore was a mere 100 kilometers to the east of the synorogenic thrust front. Based upon the analyses of fossils, the $\delta^{18}O$ of the seaway was interpreted to have varied from ~–8 permil to –1 permil with eustatic and freshwater influx variations associated with expansion and contraction of the sea

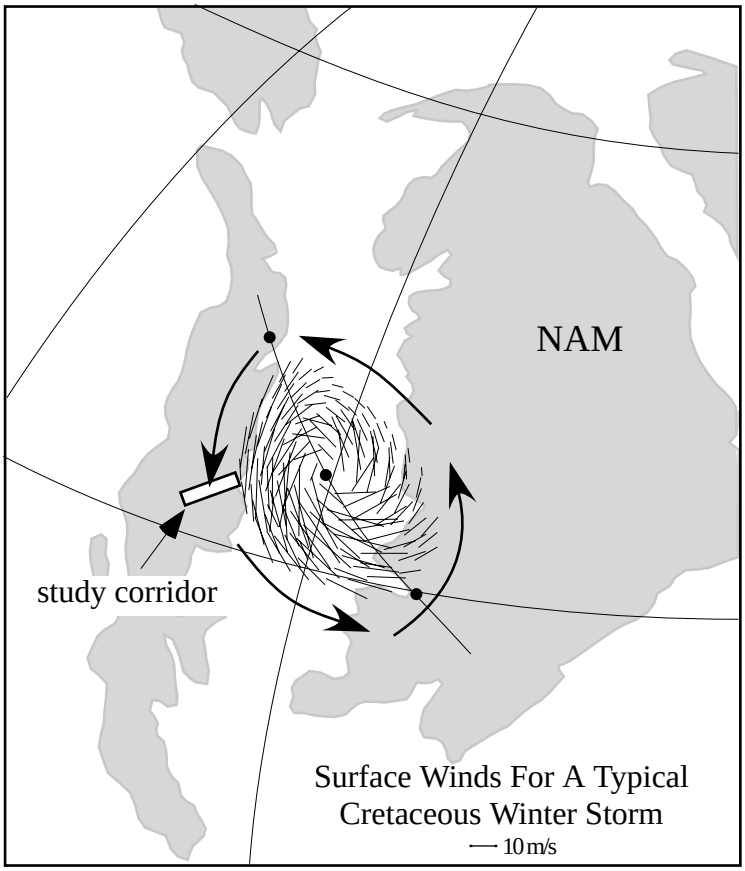

Fig. 20. Reconstruction of Western Interior Seaway during the Cretaceous including surface winds computed numerically using National Center for Atmospheric Community Climate Model for a typical extra-tropical winter storm passing west to east along the solid line with the position of the storm eye (dots) shown at 2.17, 4.14, and 6.13 days after the start of computations (modified from Slingerland and others, 1996). Proximity of the study corridor to coastal precipitation is also shown.

(Cadrin and others, 1995; Jewell, 1996). Thus, the $\delta^{18}O$ of the nearshore meteoric water could have been somewhat lower than the range expected for open oceans with a $\delta^{18}O$ of 0 permil. Cretaceous climate reconstructions predict high rainfall and seaway-derived precipitation from winter storm systems adjacent to the Montana recess (fig. 20; Ericksen and Slingerland, 1990; Slingerland and others, 1996). The availability of coastal rainfall sourced from the interior seaway makes it unnecessary to invoke buffering by regional fluid-rock interaction of far traveled, isotopically evolved precipitation to produce late-stage vein calcite values near and below 0 permil (for example, Nesbitt and Muehlenbachs, 1995).

The inferred infiltration of Lost River Range deformed zones and veins and Tendoy Range veins by extra-basinal fluids, could provide a mechanism for the metasomatism observed in the deformation zones. A geometrically necessary décollement in the Antler flysch (McGowen Creek Formation), ~600 meters below Willow Creek anticline, is a possible source for the Si, K, and Al enrichment of the Mississippian carbonates, if fluid flow into the rocks now exposed at Willow Creek occurred through imbricate faults in communication with the décollement. Alternatively, in a

less likely scenario, surface-derived fluids could have leached these elements from now eroded, structurally-higher lithologies during up-temperature fluid flow to greater depths, now represented by the Willow Creek exposures. The inferred addition of surficial fluids to depths of 7 to 10 kilometers in the thrust belt implies a fluid regime involving significant topographically driven recharge. Price (2001) and Osatedz and others (2002) attributes deep penetration (>8 km) of meteoric fluids with advective cooling of the hanging wall and footwall of the Lewis thrust sheet and the diachronous foreland-migrating Late Cretaceous chemical remagnetization of Devonian and Mississippian carbonates observed throughout the Front Ranges of the Canadian Rocky Mountains (Enkin and others, 2000), a few 100 kilometers north of the Montana recess. Numerical simulations of fluid flow in orogenic belts by Koons and Craw (1991) and Ge and Garven (1994) predict topographically driven deep penetration of meteoric fluids, then buoyant flow, up dip and towards the foreland. Fluid-rock interactions are expected to be complex in orogenic belts, and to vary as a function of topographic evolution, deformation history affecting permeability, fluid chemistry, and environmental conditions along protracted flow paths.

Eocene synkinematic calcite, associated with the Idaho batholith (Criss and Taylor, 1983), Pioneer core complex breccias (Bebout and others, 2001), and extensional veins and cataclasites within the Lost River (Bebout and others, 2001) and Tendoy Ranges (Johnson, ms, 2002; A. Johnson, D. Anastasio, and G. Bebout, manuscript in preparation), records exchange with more ^{18}O-depleted fluids. Calculated $\delta^{18}O$ for these fluids are in the range of –19 permil to –13 permil for a range of deformation temperatures from hinterland to foreland and the fluids are believed to have had meteoric sources. The calculated $\delta^{18}O$ values for these fluids are similar to values near –16 permil estimated by Criss and Taylor (1983) for aqueous fluids that produced hydrothermal zones adjacent to hypabyssal Eocene instrusives in central Idaho. The transition from a Cretaceous hydrogeologic regime influenced by the Western Interior Seaway to one characterized by more inland meteoric waters with lower $\delta^{18}O$ is consistent with the evolution of Tertiary paleogeography in the northern Rockies, including thrust wedge emergence and seaway retreat (Bebout and others, 2001).

CONCLUSIONS

Folding at Willow Creek anticline, Lost River Range, Idaho resulted in cleavage development in thin deformation zones, separated by massive, mildly deformed carbonates. Strain magnitudes range from $\bar{e}_s$=0.32 (1.15:0.93:0.73) in massive layers to $\bar{e}_s$=0.64 (1.29:0.80:0.52) in deformation zones. There is a positive linear correlation between strain and volume loss, which ranges from –12 percent to –49 percent at a cubic centimeter scale. Cleavage selvages are depleted in Ca and $\delta^{18}O$ and enriched in other elements (particularly Si, Al, and K) relative to microlithons and protolith carbonates. Mass balance considerations indicate that cleavage was formed by incongruent pressure solution leading to a passive concentration of less soluble components during Ca-CO_2 (calcite) loss and metasomatic additions on Si, Al, and K to produce increased abundances of clay minerals. Metasomatic strain softening enhanced deformation zone development and permeability. Stable isotope data show that fluid infiltration was heterogeneous at a fine scale and resulted from positive feedback between deformation and infiltration by far-traveled surficial fluids. Increased fluid infiltration and isotopic exchange in deformation zones was associated with volume loss, prolate strains, and crystallization of clays, which define cleavage selvages. Mass transfer was accommodated by diffusion early and advection later in the deformation history. Mesoscopic structures (for example, deformation zones, faults, veins) focused fluid flow and were kinematically related to larger-scale thrust and fold structures. The inferred infiltration of surficial fluids to depths of 7 to 10 kilometers implies significant topographically driven recharge. Deformed whole rocks and microsamples are lower

in $\delta^{18}O$ than undeformed samples, which have O- and C-isotope values similar to those of marine carbonates. Veins are even lower in $\delta^{18}O$ with minimum values of +5 to +10 permil reflecting penetration of the thrust wedge by ocean-derived precipitation, consistent with Cretaceous reconstructions of the Western Interior Seaway.

ACKNOWLEDGMENTS

This study was supported by National Science Foundation grant EAR-9405626 awarded to Anastasio and Bebout. Martin Burkhart, Nick Oliver, and Zach Sharp are thanked for providing thorough reviews of the manuscript for the journal.

References

Ague, J. J., 1991, Evidence for major mass transfer and volume strain during regional metamorphism of pelites: Geology, v. 19, p. 855-858.

——— 1994, Mass transfer during Barrovian metamorphism of pelites, south-central Connecticut, I: Evidence for composition and volume change: American Journal of Science, v. 294, p. 989-1057.

Allmendinger, R. W., 1992, Fold and thrust tectonics of the western United States exclusive of the accreted terranes, *in* Burchfiel, B. C., Lipman, P. W., and Zoback, M. L., editors, Cordilleran Orogen: conterminous United States: Geological Society of America, G-3, p. 583-607.

Alvarez, W., Engelder, T., and Geiser, P. A., 1978, Classification of solution cleavage in pelagic limestones: Geology, v. 6, p. 263-266.

Anastasio, D. J., Fisher, D. M., Messina, T. A., and Holl, J. E., 1997, Kinematics of Décollement folding in the Lost River Range, Idaho: Journal of Structural Geology, v. 19, p. 355-368.

Anastasio, D. J., Harkins, N. W., Latta, D. K., Ashcroft, J., 2002, Coeval, in- and out-of-sequence deformation within the Frontal Thrust Sheets of the Tendoy Mountains, SW Montana: Geological Society of America, Abstracts with Programs, v. 34, p. A-7.

Anders, M. H., Rodgers, D. W., and Hagstrum, J. T., 1993, The growth of fault-bounded tilt blocks: Tectonics, v. 12, p. 1451-1459.

Bachu, S., 1995, Synthesis and model of formation-water flow, Alberta Basin, Canada: Bulletin of the American Association of Petroleum Geologists, v. 79, p. 1159-1178.

Beach, A., 1977, Vein arrays, hydraulic fractures and pressure-solution structures in a deformed flysch sequence, S.W. England: Tectonophysics, v. 40, p. 201-225.

Bebout, G. E., Anastasio, D. J., and Holl, J.E., 2001, Synorogenic crustal fluid infiltration in the Idaho-Montana thrust belt: Geophysical Research Letters, v. 28, p. 4295-4298.

Bell, A. M., 1985, Strain paths during slaty cleavage formation-the role of volume loss: Journal of Structural Geology, v. 7, p. 563-568.

Bethke, C. M., and Marshak, S., 1990, Brine migrations across North America—the plate tectonics of groundwater: Annual Reviews of Earth and Planetary Science, v. 18, p. 287-315.

Beutner, E. C., ms, 1968, Structure and tectonics of the southern Lemhi Range, Idaho: Ph. D. thesis, Pennsylvania State University, University Park, Pennsylvania, 106 p.

Beutner, E. C., and Charles, E. G., 1985, Large volume loss during cleavage formation, Hamburg sequence: Geology, v. 13, p. 803-805.

Burkhard, M., 1990, Ductile deformation mechanisms in micritic limestones naturally deformed at low temperatures (150-350°C), *in* Knipe, R. J., and Rutter, E. H., editors, Deformation Mechanisms, Rheology and Tectonics: Geologic Society of London Special Publication, v. 54, p. 241-257.

Cadrin, A. A. J., Kyser, T. K., Caldwell, W. G. E., and Longstaffe, F. J., 1995, Isotopic and chemical compositions of bentonites as paleoenvironmental indicators of the Cretaceous Western Interior Seaway: Palaeogeography, Palaeoclimatology, and Palaeoecology, v. 119, p. 301-320.

Caine, J. Saul, Evans, J. P., and Forester, C. B., 1996, Fault zone architecture and permeability structure: Geology, v. 24, p. 1025-1028.

Carson, B., and Screaton, E. J., 1998, Fluid flow in accretionary prisms; evidence for focused, time-variable discharge: Reviews of Geophysics, v. 36, p. 329-351.

Clifford, P. M., Rice, M. C., Pryer, L. L, and Fueten, F., 1987, Mass transfer in unmetamorphosed carbonates and during low-grade metamorphism of arenites *in* Jones, M. E., and Preston, R. M. F., editors, Deformation of sediments and sedimentary rocks: Geological Society of London Special Publication, v. 29, p. 197-209.

Cox, S. F., and Etheridge, M. A., 1989, Coupled grain-scale dilatancy and mass transfer during deformation at high fluid pressures; examples from Mount Lyell, Tasmania: Journal of Structural Geology, v. 11, p. 147-162.

Criss, R. E., and Taylor, H. P., Jr., 1983, An $^{18}O/^{16}O$ and D/H study of Tertiary hydrothermal systems in the southern half of the Idaho batholith: Bulletin of the Geological Society of America, v. 94, p. 640-663.

Criss, R. E., Champion, D. E., and McIntyre, D. H., 1985, Oxygen isotope, aeromagnetic, and gravity anomalies associated with hydrothermally altered zones in the Yankee Fork mining district, Custer County, Idaho: Economic Geology, v. 80, p. 1277-1296.

Criss, R. E., Fleck, R. J., and Taylor, H. P., Jr., 1991, Tertiary meteoric hydrothermal systems and their relation to ore deposition, northwestern United States and southern British Columbia: Journal of Geophysical Research, v. 96, p. 13,335-13,356.

Crone, A. J., and Machette, M. N., 1984, Surface faulting accompanying the Borah Peak earthquake, central Idaho: Geology, v. 12, p. 664-667.
Davidson, S., Anastasio, D. J., and Bebout, G. E., 1998, Volume strain associated with cleavage development in carbonate rocks, Lost River Range, Idaho: Journal of Structural Geology, v. 20, p. 707-726.
Davis, D., Suppe, J., and Dahlen, J. A., 1983, Mechanics of fold and thrust belts and accretionary wedges: Journal of Geophysical Research, v. 88, p. 1153-1172.
DePaor, D. G., 1993, R_f/Fry 5.1 Bundle: Baltimore, Maryland, Earth'nWare, Inc.
DePaor, D. G., Simpson, C., Bailey, C. M., McCaffrey, K. J. W., Beam, E., Gower, R. J. W., and Aziz, G., 1991, The role of solution in the formation of boudinage and transverse veins in carbonate rocks at Rheems, Pennsylvania: Bulletin of the Geological Society of America, v. 103. p. 1552-1563.
DePrang, A. B., ms, 1997, A geological and geophysical investigation of Cenozoic extensional deformation in the Pioneer metamorphic core complex, south central Idaho: M.S. thesis, University of New Orleans, New Orleans, Louisiana, 69 p.
Dover, J. H., 1981, Geology of the Boulder-Pioneer wilderness study area, Blaine and Custer counties, Idaho: United states Geological Survey Bulletin, v. 1497-A, p. 21-75.
Duane, M. J., and de Wit, M. J., 1988, Pb-Zn ore deposits of the northern Caledonides—products of continental-scale fluid mixing and tectonic expulsion during continental collision: Geology, v. 16, p. 999-1002.
Dunnet, D., 1969, A technique of finite strain analysis using elliptical particles: Tectonophysics, v. 7, p. 117-1365.
Durney, D. W., 1972, Solution-transfer, an important geological deformation mechanism: Nature, v. 235, p. 315-317.
Durney, D.W., and Ramsay, J. G., 1973, Incremental strains measured by syntectonic crystal growths *in* DeJong, K. A., and Scholten, R., editors, Gravity and Tectonics: New York, John Wiley and Sons, p. 67-98.
Elliott, D., 1973. Diffusion flow laws in metamorphic rocks: Bulletin of the Geological Society of America, v. 84, p. 2645-2664.
——— 1976, The energy balance and deformation mechanisms of thrust sheets: Philosophical Transactions of the Royal Society of London, v. 283, p. 289-312.
Engelder, T., 1984, The role of pore water circulation during the deformation of foreland fold and thrust belts: Journal of Geophysical Research, v. 89, p. 4319-4325.
Engelder, T., and Engelder, R., 1977, Fossil distortion and décollement tectonics of the Appalachian Plateau: Geology, v. 5, p. 457-460.
Engelder, T., and Marshak, S., 1985, Disjunctive cleavage formed at shallow depths in sedimentary rocks: Journal of Structural Geology, v. 7, p. 327-343.
Enkin, R. J., Osadetz, K. G., Baker, J., and Kisilevsky, D., 2000, Orogenic remagnetizations in the front ranges and inner foothills of the southern Canadian Cordillera; chemical harbinger and thermal handmaiden of Cordilleran deformation: Bulletin of the Geological Society of America, v. 112, p. 929-94.
Ericksen, M. C., and Slingerland, R. L., 1990, Numerical simulations of tidal and wind-driven circulation in the cretaceous interior seaway of North America: Bulletin of the Geological Society of America, v. 102, p. 1499-1516.
Erslev, E. A., 1988, Normalized center-to-center strain analysis of packed aggregates: Journal of Structural Geology, v. 10, p. 201-209.
——— 1989, Instrain an integrated fabric analysis program for the Macintosh®: Fort Collins, Colorado, Colorado State University.
Erslev, E. A., and Ge, H., 1990, Least-squares center-to-center and mean object ellipse fabric analysis: Journal of Structural Geology, v. 12, p. 1047-1059.
Erslev, E. A., and Mann, C., 1984, Pressure solution shortening in the Martinsburg Slate, New Jersey: Proceedings of the Pennsylvania Academy of Science, v. 58, p. 84-88.
Erslev, E. A., and Ward, D. J., 1994, Non-volatile element and volume flux in coalesced slaty cleavage: Journal of Structural Geology, v. 16, p. 531-553.
Evans, M. A., and Battles, D. A., 1999, Fluid inclusion and stable isotope analyses of veins from the central Appalachian Valley and Ridge province: implications for regional synorogenic hydrologic structure and fluid migration: Bulletin of the Geological Society of America, v. 111, p. 1841-1860.
Feehan, J. G., and Brandon, M. T., 1999, Contribution of ductile flow to exhumation of low T-high P metamorphic rocks: San Juan-Cascade nappes, NW Washington State: Journal of Geophysical Research, v. 104, p. 10,883-10,902.
Fisher, D. M., and Anastasio, D. J., 1994, Kinematic analysis of a large-scale leading edge fold, Lost River Range, Idaho, U.S.A.: Journal of Structural Geology, v. 16, p. 571-584.
Fisher, D. M., and Brantley, S. L., 1992, Models of quartz overgrowth and vein formation: deformation and episodic fluid flow in an ancient subduction zone: Journal of Geophysical Research, v. 97, p. 20,043-20,061.
Forster, C., and Smith, L., 1990, Fluid flow in tectonic regimes, *in* Nesbitt, B. E., editor, Short Course on Fluids in Tectonically Active Regimes of the Continental Crust: Mineralogical Association of Canada Short Course Handbook, v. 18, p. 1-47.
Fry, N., 1979, Random point distributions and strain measurement in rocks: Tectonophysics, v. 60, p. 806-807.
Garven, G., 1989, A hydrogeologic model for the formation of the giant oil sands deposits of the Western Canada sedimentary basin: American Journal of Science, v. 289, p. 105-166.
Ge, S., and Garven, G., 1994, A theoretical model for thrust-induced deep groundwater expulsion with application to the Canadian Rocky Mountains: Journal of Geophysical Research, v. 99, p. 13851-13868.
Geiser, P. A., 1974, Cleavage in some sedimentary rocks of the central Valley and Ridge Province, Maryland: Bulletin of the Geological Society of America, v. 85, p. 1399-1412.
Goldstein, A., Pickens, J., Klepeis, K., and Linn, F., 1995, Finite strain heterogeneity and volume loss in slates of the Taconic allochton, Vermont, U.S.A.: Journal of Structural Geology, v. 17, p. 1207-1216.

Gray, D. R., 1978, Cleavages in psammitic rocks from southeastern Australia: Their nature and origin: Bulletin of the Geological Society of America, v. 89, p. 577-590.
Groshong, R. H., 1975, Strain, fractures, and pressure solution in natural single layer folds: Bulletin of the Geological Society of America, v. 86, p. 1363-1376.
Harkins, N. W., Latta, D. K., Anastasio, D. J., and Pazzaglia, F. J., 2004a, Surficial and bedrock geologic map of the Dixon Mountain 7.5′ quadrangle, southwest Montana: Montana Bureau of Mines and Geology Open File Report 495, scale 1:24,000, text 12 p., 2 pl.
Harkins, N. W., Newton, M., Anastasio, D. J., and Pazzaglia, F. J., 2004b, Bedrock and surficial geologic map of the Caboose Canyon 7.5′ quadrangle, southwest Montana: Montana Bureau of Mines and Geology Open File Report 494, scale 1:24,000, text 14 p., 2 pl.
Hedlund, C. A., Anastasio, D. J., and Fisher, D. M., 1994, Kinematics of Fault-Related Folding in a Duplex, Lost River Range, Idaho, U.S.A.: Journal of Structural Geology, v. 16, p. 571-584.
Henderson, J. R., Wright, T., and Henderson, M. N., 1986, A history of cleavage and folding: An example from the Goldenville Formation, Nova Scotia: Bulletin of the Geological Society of America, v. 97, p. 1354-1366.
Holl, J. E., and Anastasio, D. J., 1995, Cleavage development within a foreland fold and thrust belt, southern Pyrenees, Spain: Journal of Structural Geology, v. 17, p. 357-369.
Hubbert, M. K., and Rubey, W. W., 1959, Role of fluid pressure in mechanics of overthrust faulting. I. mechanics of fluid-filled porous solids and its application to overthrust faulting: Bulletin of the Geological Society of America, v. 70, p. 115-166.
Hutcheon, I., Cody, J., and Yang, C., 2000, Fluid flow in the western Canadian sedimentary basin-a biased perspective based on geochemistry, *in* Kyser, K., editor, Fluids and Basin Evolution: Mineralogical Association of Canada Short course series, v. 28, p. 197-210.
Jamison, W. R., and Spang, J. H., 1976, Use of calcite lamellae to infer differential stress: Bulletin of the Geological Society of America, v. 87, p. 868-872.
Janecke, S. U., 1992, Kinematics and timing of three superimposed extensional systems, east central Idaho: evidence for an Eocene tectonic transition: Tectonics, v. 11, p. 1121-1138.
Janecke, S. U., and Snee, L. W., 1993, Timing and episodicity of middle Eocene volcanism and onset of conglomerate deposition, Idaho: Journal of Geology, v. 101, p. 603-621.
Janecke, S. U., and Wilson, E., 1992, Geologic map of Borah Peak, Burnt Creek, Elkhorn Creek, and Leatherman Pass 7.5 minute quadrangles, Custer and Lemhi Counties, Idaho: Idaho Geologic Survey, Technical Report 92-5, Moscow, Idaho, scale 1:24,000.
Janecke, S. U., Geissman, J. W., and Bruhn, R. L., 1991, Localized rotation during Paleogene extension in east central Idaho: paleomagnetic and geologic evidence: Tectonics, v. 10, p. 403-432.
Jewell, P. W., 1996, Circulation, salinity, and dissolved oxygen in the Cretaceous North American seaway: American Journal of Science, v. 296, p. 1093-1125.
Johnson, A. C., ms, 2002, Syntectonic fluid-rock interactions involving surficial waters in the Sevier thrust belt, Tendoy Mountains, southwest Montana: M.S. thesis, Lehigh University, Bethlehem, Pennsylvania, 62 p.
Kalakay, T. J., ms, 2001, The role of magmatism during crustal shortening in the Sevier retroarc fold-and-thrust belt of southwest Montana: Ph.D. thesis, University of Wyoming, Laramie, Wyoming.
Kendall, C., Skalsh, M. M. G., and Bullen, T. D., 1995, Isotope tracers of water and solute sources in catchments *in* Trudgill, S. T., editor, Solute Modeling in Catchment Systems: New York, John Wiley and Sons, Ltd., p. 261-303.
Kerrich, R., 1986, Fluid infiltration into fault zones: chemical, isotopic, and mechanical effects: Pure and Applied Geophysics, v. 124, p. 225-268.
Knipe, R. J., 1989, Deformation mechanisms; recognition from natural tectonites: Journal of Structural Geology, v. 11, p. 127-146.
Koons, P. O., and Craw, D., 1991, Evolution of fluid driving forces and compression within collisional orogens: Geophysical Research Letters, v. 18, p. 935-938.
Kulik, D. M., and Perry, W. J., Jr., 1988, The Blacktail-Snowcrest foreland uplift and its influence on structure of the Cordilleran thrust belt-geological and geophysical evidence for the overlap province in southwestern Montana, *in* Schmidt, C. J., and Perry, W. J., Jr., editors, Interactions of Rocky Mountain foreland and Cordilleran thrust belt: Geological Society of America Memoir 171, p. 291-306.
Latta, D. K., and Anastasio, D. J., 2000, Emergent Faulting and Growth Strata in the Sevier Hinterland Idaho: a Record of Coeval Compression and Extension in the Early Eocene: GeoCanada 2000, Millennium Geoscience Summit, Extended abstract with figures, Conference CD and www.geocanada2000.com171, p. 291-306.
Link, P. K., Skipp, B., Hait, M. H., Jr., Janecke, S. U., and Burton, B. R., 1988, Structural and stratigraphic transect of south-central Idaho: a field guide to the Lost River, White Knob, Pioneer, Boulder, and Smoky Mountains, *in* Link, P. K., and Hackett, W. R., editors, Guidebook to the Geology of Central and Southern Idaho: Idaho Geological Survey Bulletin, v. 27, p. 5-42.
Lonn, J. D., Skipp, B., Ruppel, E. T., Janecke, S. U., Perry, W. J., Sears, J. W., Bartholomew, M. J., Stickney, M. C., Fritz, W. J., Hurlow, H. A., and Thomas, R. C., 2000, Geologic map of the Lima 30′ x 60′ Quadrangle, Southwest Montana: Montana Bureau of Mines and Geology open file report 408, scale 1:100,000.
Lowell, W. R., 1965, Geologic map of the Bannack-Grayling area, Beaverhead County, Montana: U.S. Geological Survey Miscellaneous Geologic Investigations Map I-433, scale 1:24,000.
Machel, H. G., Cavell, P. A., and Patey, K. S., 1996, Isotopic evidence for carbonate cementation and recrystallization, and for tectonic expulsion of fluids into the Western Canada Sedimentary Basin: Bulletin of the Geological Society of America, v. 108, p. 1108-1119.
Machel, H. G., Buschkuehle, B. E., and Michael, K., 2002, Evidence for squeegee flow in the Rocky Mountain Foreland basin: Extended abstract AAPG Hedberg Conference Deformation History, Fluid Flow Reconstruction and Reservoir Appraisal in Foreland Fold and Thrust Belts, 4 p.

Mamet, B. L., Skipp, B., Sando, W. J., and Mapel, J., 1971, Biostratigraphy of upper Mississippian and associated Carboniferous rocks in south central Idaho: Bulletin of the American Association of Petroleum Geologists, v. 55, p. 20-33.
Mapel, W. J., Reed, W. H., and Smith, R. K., 1965, Geologic map and sections of the Double Springs Quadrangle, Custer and Lemhi Counties: Idaho, USGS Map GQ464, scale 1:62,500.
Marshak, S., and Engelder, T., 1985, Development of cleavage in limestones of a fold-thrust belt in New York: Journal of Structural Geology, v. 7, p. 345-359.
McCrea, J. M., 1950, The isotopic chemistry of carbonates and a paleotemperature scale: Journal of Chemical Physics, v. 18, p. 849-857.
Means, W. D., 1975, Natural and experimental microstructures in deformed micaceous sandstones: Bulletin of the Geological Society of America, v. 86, p. 1221-1229.
Messina, T. A., ms, 1993, The geometry and kinematics of intra-thrust sheet décollement folding: Lost River Range, Idaho: M.S. thesis, Lehigh University, Bethlehem, Pennsylvania, 50 p.
Meyer, T. J., and Dunne, W. M., 1990, Deformation of Helderberg limestones above the blind thrust system of the Central Appalachians: Journal of Geology, v. 98, p. 108-117.
Mitra, S., 1976, A quantitative study of deformation mechanisms and finite strain in quartzite: Contributions to Mineralogy and Petrology, v. 59, p. 203-226.
——— 1987, Regional variations in deformation mechanisms and structural styles in the central Appalachian orogenic belt: Geological Society of America Bulletin, v. 98, p. 569-590.
Nadai, A., 1963, Theory of flow and fracture of solids, volume 2: New York, McGraw-Hill, 705 p.
Nesbitt, B. E., and Muehlenbachs, K., 1991, Stable isotope constraints on the nature of the syntectonic fluid regime of the Canadian Cordillera: Geophysical Research Letters, v. 18, p. 963-966.
——— 1995, Geochemical studies of the origins and effects of synorogenic crustal fluids in the southern Omineca Belt of British Columbia, Canada: Bulletin of the American Geological Society, v. 107, p. 1033-1050.
Newman, J., 1994, The influence of grain size and grain size distribution on methods for estimating paleostresses from twinning in carbonates: Journal of Structural Geology, v. 16, p. 1589-1601.
Nickelson, R. P., 1972, Attributes of rock cleavage in some mudstones and limestones of the Valley and Ridge province, Pennsylvania: Proceedings of the Pennsylvania Academy of Science, v. 46, p. 107-112.
Oliver, J., 1986, Fluids expelled tectonically from orogenic belts: their role in hydrocarbon migration and other geologic phenomena: Geology, v. 14, p. 99-102.
O'Neil, J. R., Clayton, R. N., and Mayeda, T. K., 1969, Oxygen isotope fractionation in divalent metal carbonates: Journal of Chemical Physics, v. 51, p. 5547-5558.
O'Neill, R. L., ms, 1985, Superposition of Cenozoic extension on Mesozoic compressional structures in the Pioneer Mountains, central Idaho: MS thesis, Lehigh University, Bethlehem, Pennsylvania, 59 p.
O'Neill, R. L., and Pavlis, T. L., 1988, Superposition of Cenozoic extension on Mesozoic compressional structures in the Pioneer Mountains metamorphic core complex, central Idaho: Bulletin of the Geological Society of America, v. 100, p. 1833-1845.
Osadetz, K. G., Kohn, B. P., Feinstein, S., and Price, R. A., 2002, Constraining foreland belt thermal history using apatite fission track thermochronology and organic maturity: implications for Lewis Thrust, Flathead Fault and Waterton gas field in the southern Canadian Cordillera, *in* Roure, F., and Swennen, R., editors, Deformation History, Fluid Flow Reconstruction and Reservoir Appraisal in Foreland Fold and Thrust Belts, Abstract Volume: American Association of Petroleum Geologists' Institut Francais du Petrole Hedberg Research Conference, May 14-18, 2002, Palermo-Mondello, Italy, p. 37a-37d.
Peach, C. J., and Lisle, R. J., 1979, A Fortran IV program for the analysis of tectonic strain using deformed elliptical markers: Computers & Geosciences, v. 5, p. 325-334.
Perry, W. J., and Sando, W. J., 1983, Sequence of deformation of Cordilleran thrust belt in Lima, Montana region, *in* Powers, R. B., editor, Geologic studies of the Cordilleran thrust belt: Denver, Colorado, Rocky Mountain Association of Geologists, p. 137-144.
Perry, W. J., Jr., Wardlaw, B. R., Bostick, N. H., and Maughan, E. K., 1983, Structure, burial history, and petroleum potential of the frontal thrust belt and adjacent foreland, southwest, Montana: Bulletin of the American Association of Petroleum Geologists, v. 67, p. 725-743.
Perry, W. J., Jr., Haley, J. C., Nichols, D. J., Hammons, P. M., and Ponton, J. D., 1988, Interactions of Rocky Mountain foreland and Cordilleran thrust belt in Lima region, southwest Montana, *in* Schmidt, C. J., and Perry, W. J., Jr., editors, Interactions of Rocky Mountain foreland and Cordilleran thrust belt: Geological Society of America Memoir 171, p. 267-290.
Plessman, W., 1965, Gesteinslosung, ein Hauptfaktor beim Schieferungsprozess: Geologische Mitteilungen, v. 4, p. 69-82.
Price, R. A., 2001, Deep refrigeration of an evolving thrust and fold belt by enhanced penetration of meteoric water: the Lewis thrust sheet, southern Canadian Rocky Mountains: Geological Society of America, Abstracts with Programs, v. 33, p. A-52.
Ramsay, J. G., 1967, Folding and Fracturing of Rocks: New York, McGraw-Hill, 555 p.
——— 1980, Shear zone geometry: a review: Journal of Structural Geology, v. 2, p. 83-89.
Ramsay, J. G., and Huber, Martin I., 1983, The Techniques of Modern Structural Geology, v. 1: Strain Analysis: London, Academic Press, Inc., 307 p.
Ramsay J. G., and Wood, D. S., 1973, The geometric effects of volume change during deformation processes: Tectonophysics, v. 16, p. 263-277.
Rodgers, D. W., and Janecke, S. U., 1992, Tertiary paleogeologic maps of the western Idaho-Wyoming-Montana thrust belt, *in* Link, P. K., Kuntz, M. A., and Platt, L. B., editors, Regional Geology of Eastern Idaho and Western Wyoming: Geological Society of America Memoir 179, p. 83-94.
Ross, C. P., 1947, Geology of Borah Peak quadrangle, Idaho: Bulletin of the Geological Society of America, v. 58, p. 1085-1160.

Rowan, M. G., 1991.Three-dimensional finite strain from crinoid ossicles: Journal of Structural Geology, v. 13, p. 1049-1059.
Ruppel, E. T., and Lopez, D. A., 1984, The thrust belt in southwest Montana and east-central Idaho: U.S. Geological Survey Professional Paper, 1278, 41 p.
Rutter, E. H., 1976, The kinetics of rock deformation by pressure solution: London, Philosophical Transactions of the Royal Society, v. 283, p. 203-220.
——— 1983, Pressure solution in nature, theory and experiment: London, Journal of the Geological Society, v. 140, p. 725-740.
Rye, D. M., and Bradbury, H. J., 1988, Fluid flow in the crust: an example from a Pyrenean thrust ramp: American Journal of Science, v. 288, p. 197-235.
Schmitt, J. G., Haley, J. C., Lageson, D. R., Horton, B. K., and Azevedo, P. A., 1995, Sedimentology and tectonics of the Bannack-McKnight Canyon-Red Butte area, southwest Montana: new perspectives on the Beaverhead Group and Sevier orogenic, belt, *in* Mogk, D. W., editor, Northwest Geology. Field guide to the geologic excursions in southwest Montana: Bozeman, Montana, Geological Society of America Annual Meeting, Rocky Mountain Section, v. 24, p. 245-313.
Schweitzer, J., and Simpson, C., 1986, Cleavage development in dolomite of the Elbrook Formation, southwest, Virginia: Bulletin of the Geological Society of America, v. 97, p. 778-786.
Sheppard, S. M. F., Nielsen, R. L., and Taylor, H. P., 1969, Oxygen and hydrogen isotope ratios of clay minerals from porphyry copper deposits: Economic Geology and the Bulletin of the Society of Economic Geologists, v. 64, p. 755-777.
Sherwood, E. R., ms, 1994, Remagnetization of the Scott Peak Formation associated with Tertiary igneous activity: a comparative study of two deformed carbonate structures in the Lost River Range, Idaho: M.S. thesis, Lehigh University, Bethlehem, Pennsylvania, 73 p.
Sibson, R. H., 1981, Fluid flow accompanying faulting: field evidence and models, *in* Simpson, D. W., and Richards, D. G., editors, Earthquake Prediction—An International Review: American Geophysical Union, Maurice Ewing Series, v. 4, p. 593-603.
——— 1990, Conditions for fault-valve behavior, *in* Knipe, R. J., and Rutter, E. H., editors, Deformation Mechanisms, Rheology and Tectonics: Geological Society of London Publication, v. 54, p. 15-28.
Silverberg, D. S., ms, 1990, The tectonic evolution of the Pioneer Metamorphic Core Complex, South-Central Idaho: Ph. D. thesis, Massachusetts Institute of Technology, Cambridge, Massachusetts, 280 p.
Skipp, B., ms, 1985, Contraction and extension faults in the southern Beaverhead Mountains, Idaho and Montana: Ph. D. thesis, University of Colorado, Boulder, Colorado, 170 p.
Skipp, B., and Link, P. K., 1992, Middle and Late Proterozoic rocks and Late Proterozoic tectonics in the southern Beaverhead Mountains, Idaho and Montana: a preliminary report, *in* Link, P. K., Kuntz, M. A., and Platt, L. B., editors, Regional Geology of Eastern Idaho and Western Wyoming: Geological Society of America Memoir 179, p. 141-154.
Slingerland, R., Kump, L. R., Arthur, M. A., Fawcett, P. F., Sageman, B. B., and Barron, E. J., 1996, Estuarine circulation in the Turonian Western Interior Seaway of North America: Bulletin of the Geological Society of America, v. 108, p. 941-952.
Sorby, H. C., 1853, On the origin of slaty cleavage: Edinburg, New Philosophical Journal, v. 55, p. 137-148.
Spratt, D. A., ms, 1987, Finite strain and deformation mechanisms in carbonate thrust sheets: Ph. D. thesis, Johns Hopkins University, Baltimore, Maryland, 220 p.
Stephens, M. B., Glasson, M. J., and Keays, R. R., 1979, Structural and chemical aspects of metamorphic layering development in metasediments from Clunes, Australia: American Journal of Science, v. 279, p. 129-160.
Sverjensky, D. A., 1986, Genesis of Mississippi Valley-type lead-zinc deposits: Annual Reviews of Earth and Planetary Science, v. 14, p. 177-199.
Trepp, D. A., ms, 1989, Comparative petrology of pelitic and calc-silicate rocks Pioneer core complex: MS thesis, University of Oregon, Corvallis, Oregon, 95 p.
Williams, P. F., 1977, Foliation: a review and discussion: Tectonophysics, v. 39, p. 305-328.
Williams, N. S., and Bartley, J. M., 1988, Geometry and sequence of thrusting, McKnight and Kelmbeck canyons, Tendoy Range, southwestern Montana, *in* Schmidt, C. J., and Perry, W. J., Jr., editors, Interactions of Rocky Mountain foreland and Cordilleran thrust belt: Geological Society of America Memoir 171, p. 307-318.
Wilson, A. B., and Skipp, B., 1994, Geologic map of the eastern part of the Challis National Forest and vicinity, Idaho: U.S. Geological Survey, Miscellaneous Investigation Series, Map I-2396, scale 1: 250,000.
Wintsch, R. P., Kvale, C. M., and Kisch, H. J., 1991, Open-system constant volume development of slaty cleavage, and strain induced replacement reactions in the Martinsburg Formation, Lehigh Gap, Pennsylvania: Bulletin of the Geological Society of America, v. 103, p. 916-927.
Wright, T. O., and Henderson, J. R., 1992, Volume loss during cleavage formation in the Meguma Group, Nova Scotia, Canada: Journal of Structural Geology, v. 14, p. 281-290.
Wright, T. O., and Platt, L. B., 1982, Pressure dissolution and cleavage in the Martinsburg Shale: American Journal of Science, v. 282, p. 122-135.
Wust, S. L., and Link, P. K., 1988, Field guide to the Pioneer Mountains core complex, south-central Idaho, *in* Link, P. K., and Hackett, W. R., editors, Guidebook Geology Central and Southern Idaho: Idaho Geological Survey Bulletin, v. 27, p. 43-54.
Yonkee, W. A., Parry, W. T., and Bruhn, R. L., 2003, Relations between progressive deformation and fluid rock interaction during shear-zone growth in a basement-cored thrust sheet, Sevier orogenic belt, Utah: American Journal of Science, v. 303, p. 1-59.